

METHYL ACETATE AND ITS SINGLY DEUTERATED ISOTOPOMERS IN THE INTERSTELLAR MEDIUM

ANKAN DAS¹, LITON MAJUMDAR^{2,3,1}, DIPEN SAHU¹, PRASANTA GORAI¹, B SIVARAMAN⁴, SANDIP K. CHAKRABARTI^{5,1}

¹Indian Centre for Space Physics, Chalantika 43, Garia Station Rd., Kolkata, 700084, India.

²Univ. Bordeaux, LAB, UMR 5804, F-33270 Floirac, France.

³CNRS, LAB, UMR 5804, F-33270 Floirac, France.

⁴Space and Atmospheric Sciences Division, Physical Research Laboratory, Ahmedabad, 380009, India. and

⁵S. N. Bose National Centre for Basic Sciences, Salt Lake, Kolkata, 700098, India.

Draft version April 4, 2024

ABSTRACT

Methyl acetate ($\text{CH}_3\text{COOCH}_3$) has been recently observed by IRAM 30 m radio telescope in Orion though the presence of its deuterated isotopomers is yet to be confirmed. We therefore study the properties of various forms of methyl acetate, namely, $\text{CH}_3\text{COOCH}_3$, $\text{CH}_2\text{DCOOCH}_3$ and $\text{CH}_3\text{COOCH}_2\text{D}$. Our simulation reveals that these species could be produced efficiently both in gas as well as in ice phases. Production of methyl acetate could follow radical-radical reaction between acetyl (CH_3CO) and methoxy (CH_3O) radicals. To predict abundances of $\text{CH}_3\text{COOCH}_3$ along with its two singly deuterated isotopomers and its two isomers (ethyl formate and hydroxyacetone), we prepare a gas-grain chemical network to study chemical evolution of these molecules. Since gas phase rate coefficients for methyl acetate and its related species were unknown, either we consider similar rate coefficients for similar types of reactions (by following existing data bases) or we carry out quantum chemical calculations to estimate the unknown rate coefficients. For the surface reactions, we use adsorption energies of reactants from some earlier studies. Moreover, we perform quantum chemical calculations to obtain spectral properties of methyl acetate in infrared and sub-millimeter regions. We prepare two catalog files for the rotational transitions of $\text{CH}_2\text{DCOOCH}_3$ and $\text{CH}_3\text{COOCH}_2\text{D}$ in JPL format, which could be useful for their detection in regions of interstellar media where $\text{CH}_3\text{COOCH}_3$ has already been observed.

Subject headings: Astrochemistry, spectra, ISM: molecules, ISM: abundances, ISM: evolution, methods: numerical

1. INTRODUCTION

According to the Cologne Database for Molecular Spectroscopy (Muller et al. 2001; Müller et al. 2005), about 180 molecules have been observed in the interstellar medium (ISM) or in circumstellar shells, among which several species are organic in nature. Several bio-molecules (amino acids) have been observed in the meteorites discovered on Earth which indicate that such complex bio-molecules must be produced in frigid and tenuous interstellar space. In fact it is long believed that basic biomolecules on earth could have been brought through numerous meteoritic bombardments in the early stage of earth's life (Oro 1961; Oro et al. 1979; Delsemme 1981). The sea water which is also produced by such bombardments (see, Sarafian et al. 2014 and references therein) should also carry complex pre-biotic species which in presence of tidal forces of the sun and the moon could have helped formation of even more complex molecules on sea surface (Chakrabarti 2012).

Quantitative computation of the abundances of complex pre-biotic molecules in collapsing clouds and star forming regions have started only recently (Chakrabarti & Chakrabarti 2000a; Chakrabarti & Chakrabarti 2000b; Chakrabarti 2015). It is suggested that even if the abundance of adenine is small enough for detection with present day technology, its immediate precursors should be observed in interstellar space (Majumdar et al. 2013). Depending

on physical conditions, these precursor molecules could be formed by various gas-grain interaction processes. Several works have been done in the past to model chemistry inside both the diffuse and dense molecular clouds (Van Dishoeck & Black 1986; Federman et al. 1995; Federman et al. 1996; Le Petit et al. 2004). A large number of models have been developed over the last few years (Hasegawa et al. 1992; Das et al. 2013a; Das et al. 2013b; Das et al. 2015; Majumdar et al. 2014a; Majumdar et al. 2014b; Das et al. 2010; Das & Chakrabarti 2011; Chakrabarti et al. 2006a; Chakrabarti et al. 2006b; Sahu et al. 2015) to explain chemical composition of interstellar gas and grains under various physical circumstances.

Methyl acetate is a flammable substance and because of the low toxicity and fast evaporation rate, it is occasionally used as a solvent (Siporska & Szydłowski 2008). It is the simplest ester and thought to be a potential prebiotic candidate which could be synthesized in the ISM easily (Senent et al. 2013). First identification of methyl acetate in the ISM was reported very recently (Tercero et al. 2013) using IRAM 30 m radio telescope towards Orion constellation. They reported the discovery of methyl acetate through the detection of large number of rotational lines from each one of the spin states of methyl acetate.

Recently, Sivaraman et al. (2013, 2015) carried out experiments to find out the spectral behaviour of methyl acetate and methyl propionate in Vacuum Ultraviolet (VUV) and Infrared (IR) at various astrophysically rel-

event temperatures (from 10 K to sublimation of ice) in ultrahigh vacuum chamber. In between 110 K to 120 K, they found an irreversible phase change (from amorphous to crystalline form of methyl acetate ice). Moreover, Sivaraman et al. (2014) carried out electron irradiation experiment on methyl acetate at 85 K to find out its dissociated products. According to their study, CO₂, CO were found to be the major products along with their by-products, such as, ethane (C₂H₆) and dimethyl ether (CH₃OCH₃). In addition, they found some CH₃OH as a by-product, which indicates the possibility of conversion from acetate to alcohol. Garrod et al. (2008) showed formation of methyl acetate in icy mantles using the gas grain warm-up chemical model. However, to our knowledge, no work has been reported till date to model deuterated forms of methyl acetate around the ISM. Here, in this paper, we are proposing to observe singly deuterated methyl acetate around the sources, where methyl acetate already been observed.

Methyl acetate is an isomer of C₃H₆O₂. It is considered to be the most abundant non-cyclic isomer of C₃H₆O₂. Among other isomers of C₃H₆O₂, hydroxyacetone (CH₃COCH₂OH) and ethyl formate (C₂H₅OCHO) are recently been observed in the ISM. Propionic acid (CH₃CH₂COOH) is also an isomer of C₃H₆O₂ and it is a plausible species in regions where acetic acid is found (Blagojevic et al. 2003). Methoxyacetaldehyde (CH₃OCH₂CHO) is another isomer which could also be observed in the ISM. Tercero et al. (2013) predicted an upper limit on column densities of propionic acid and methoxyacetaldehyde to be 1.6×10^{14} cm⁻² and 2×10^{14} cm⁻² respectively. A combined laboratory and astronomical investigation on the hydroxyacetone was conducted by Apponi et al. (2006). They derived an upper limit of 5×10^{12} cm⁻² to the column density of hydroxyacetone in Sgr B2(N) but they pointed out that it still requires further spectroscopic investigations before a decisive confirmation. Belloche et al. (2009) detected ethyl formate towards Sgr B2(N). They estimated column density of ethyl formate to be 5.4×10^{16} cm⁻². Later, Tercero et al. (2013) detected both the conformers (gauche and trans) of ethyl formate in Orion. So among various isomers of C₃H₆O₂, further laboratory and spectral survey are required for the confirmed detection of propionic acid and methoxyacetaldehyde. Ethyl formate and hydroxyacetone, detections of both being confirmed in the ISM and are included in the JPL catalog (<http://spec.jpl.nasa.gov/ftp/pub/catalog/catdir.html>).

Plan of this paper is as follows. In Section 2, chemical modeling and results are discussed. In Section 3, spectroscopical modeling are discussed and finally, in Section 4, we draw our conclusion.

2. CHEMICAL MODELING

We use our updated large gas-grain chemical network for the purpose of chemical modeling. We assume that gas and grains are coupled through accretion and thermal/non-thermal/cosmic ray evaporation processes. Details of these processes are already presented in Das et al. (2011, 2013a, 2014).

2.1. Gas phase reaction network

Here, we consider a large gas-grain chemical network to study the chemical evolution of methyl acetate along

with its two singly deuterated isotopomers. We consider 6277 gas phase reactions between 628 gas phase species. This gas phase chemical network principally adopted from UMIST 2006 (Woodall et al. 2007) database. Since this database does not consider the ortho and para spin modifications of various H bearing species and also our quantum chemical results are nuclear spin independent, we are not considering any nuclear spin states in our model. Some deuterated reactions are included by following Roberts & Millar (2000); Albertsson et al. (2013); Das et al. (2014). Moreover, we include some reactions which would eventually leads to form two singly deuterated isotopomers and some isomers of methyl acetate. This additional reactions are considered by following some earlier studies and some educated guesses. Gas phase reaction network for the formation/destruction of methyl acetate along with its deuterated isotopomers are given in Table 1. Rate coefficients for all the reactions are shown in Table 1. Here, we either use existing empirical relations for the gas phase rate coefficients or assume same rate coefficients for the reactions of comparable varieties. Rate coefficients of some reactions are calculated indigenously from our quantum chemical calculations. It is obvious that due to the zero point correction energy rate coefficients between the hydrogenated and deuterated species differ. But due to unavailability of suitable network, we assume the same reaction rates as some of the hydrogenated reactions.

Gas phase methyl acetate mainly forms in the ISM by the reaction (reaction number R1) between methoxy radical (CH₃O) and acetyl radical (CH₃CO). Electronic structure calculations are carried out by using GAUSSIAN 09W program (Foresman & Frisch 1996) to compute the rate coefficient of this reaction. DFT calculations are capable of reproducing experimental information with high reliability (Glaser et al. 2007). Here computations are performed by using Becke three-parameter Exchange and Lee, Yang and Parr correlation (B3LYP) functional (Becke 1993) with the 6-311++G(d,p) basis set available in the Gaussian 09W program. It is noticed that the difference between the sum of electronic and thermal enthalpies of products and reactants of reaction R1 is -349.657 kJ/mol. Other radical-radical reactions (reaction number R2 – R4) of methyl acetate network are also highly exothermic in nature, having, $\Delta H = -318.925$, -318.917 and -291.832 kJ/mol respectively. Thus, $\Delta H < 0$ for these reactions, which indicates that these reactions are highly exothermic in nature. Now for the highly exothermic reactions, it is expected to have no barriers even around the low temperatures (Smith 2006; Smith 2011) and it does not follow temperature dependent Arrhenius expression. There are a number of statistical treatments available for the calculation of rate coefficients of these types of reactions (Herbst 1987; Bates 1983; Wakelam et al. 2010; George et al. 2005; Bettens et al. 1995; Bass 1981). Here, we use the following semi empirical relationship developed by Bates (1983), which had been used in some earlier studies (Gupta et al. 2011; Majumdar et al. 2012):

$$K = 1 \times 10^{-21} A_r (6E_0 + N - 2)^{(3N - 7)/(3N - 7)!} \text{cm}^3 \text{s}^{-1} \quad (1)$$

where, E_0 is the magnitude of association energy in eV,

A_r ($A_r = 100$ unless better informations are available) is the transition probability (in s^{-1}) of stabilizing the transition and N is the number of nuclei in the complex ($N = 11$ for reaction no. $R1 - R4$). The upper limit set by following equation is adopted only when the calculated value from eqn. 1 exceeds the limit set by the following equation:

$$K = 7.41 \times 10^{-10} \alpha_p^{1/2} (10/\mu)^{1/2} \text{ cm}^3 \text{s}^{-1}, \quad (2)$$

where, α_p is the polarizability (we use isotropic polarizability of the largest radical having an evenly distributed charge) in \AA^3 and μ is the reduced mass of the reactants on ^{12}C amu scale as suggested by Bates (1983). In case of reaction no. (R1-R4), CH_3CO is the largest radical having $\alpha = 3.917 \text{ \AA}^3$ (Lide 2001).

Calculations of rate coefficients by eqn. 1 implies 1.19×10^{-7} , 2.25×10^{-8} , 2.24×10^{-8} and $4.70 \times 10^{-9} \text{ cm}^3 \text{s}^{-1}$ respectively for reactions $R1 - R4$ and calculations by eqn. 2 sets the upper limit of 8.44×10^{-10} , 8.37×10^{-10} , 8.37×10^{-10} and $8.44 \times 10^{-10} \text{ cm}^3 \text{s}^{-1}$ respectively for reactions $R1 - R4$. Clearly the rate coefficients calculated by eqn. 1 exceeds the limit set by eqn. 2. Thus, we are adopting only the upper limits for these reactions.

Methyl acetate could be destroyed by various types of reactions (mainly by ion-molecular reactions, and interaction with cosmic rays or with interstellar photons). Since gas-phase chemistry of cold regions are mainly dominated by exothermic ion-molecular reactions, ion-molecular pathways could serve as the dominant destruction pathways for any gas phase neutral molecules. We consider some ion molecular reactions (given in Table 1) for the destruction of $\text{CH}_3\text{COOCH}_3$ (only some dominant ions are considered). All the reactions along with their rate coefficients are shown in Table 1. Rate constants for ion-molecular reactions can be predicted by using capture theories (Herbst 2006). But $\text{CH}_3\text{COOCH}_3$ is a polar neutral species with a dipole moment 1.72 Debye. Due to the interaction between the charge and rotating permanent dipole moment, a complex situation might arise in this case. Thus, here, we use the relation developed by Su & Chesnavich (1982) to predict the rate coefficients (k_{cap}). Woon & Herbst (2009) wrote Su-Chesnavich formula in two different ways by using a parameter $x = \mu_D/\sqrt{(2\alpha_p T)}$, where k is Boltzman constant & T is the temperature. From the quantum chemical calculation, we are having polarizability of methyl acetate is 6.93 \AA . For the other isomers and deuterated forms of methyl acetate, we are considering similar α_p for our calculations.

The ion-dipole (k_{cap}) rates can be in following form;

$$k_{cap} = (0.4767x + 0.6200)k_L, \quad (3)$$

and

$$k_{cap} = [(x + 0.5090)^2 / 10.526 + 0.9754]k_L. \quad (4)$$

When $x \geq 2$, Eqn. 2 is used and when $x < 2$, Eqn. 3 is used. It clear that at $x = 0$, above relations reduce to the Langevin expression. In terms of temperature, above expression could be written alternatively into the following form. For example, when $x \geq 2$,

$$k_{cap} = c_1 + c_2 T^{-1/2}, \quad (5)$$

where, $c_1 = 0.62k_L$ and $c_2 = (0.4767\mu_D/\sqrt{2\alpha K})k_L$.

For the cosmic ray induced photo-reactions, we use following rate coefficient as used in Woodall et al. (2007),

$$k_{CR} = \alpha(T/300)^\beta \gamma / (1 - \omega), \quad (6)$$

where, α is the cosmic ray ionization rate, γ is the probability per cosmic ray ionization that the appropriate photo reaction takes place and ω is the dust-grain albedo in the far-ultraviolet. We use $\alpha = 1.30 \times 10^{-17}$ and $\omega = 0.6$ by following all other cosmic ray induced photo reactions. γ is highly sensitive to the reactants. Since no guess for this parameter was available, we choose this parameter by following cosmic ray induced photo reactions of similar types of species. For the cosmic ray induced photo reactions of HCOOCH_3 , $\gamma = 1000$ was used in Woodall et al. (2007). We use a similar choice for γ parameter while calculating the cosmic ray induced rate coefficients for $\text{CH}_3\text{COOCH}_3$ and its related species.

For the interstellar photo reactions the rate is derived by using the following relation used in Woodall et al. (2007),

$$k_{PHOTON} = \alpha \exp(-\gamma A_V) s^{-1}, \quad (7)$$

where, α is the rate in the unshielded interstellar ultraviolet radiation field and γ is used to control the increased extinction of dust at the ultraviolet wavelength. Here, we use $\alpha = 1.0 \times 10^{-9}$ and $\gamma = 1.0$. All the reaction types mentioned above are given in Table 1 for $T = 10 \text{ K}$ and $A_V = 10$.

2.2. Surface reaction network

Chemical enrichment of interstellar grain mantle solely depends on the binding energies of surface species (Das & Chakrabarti, 2011). Mobility of lighter species such as H, D, N and O mainly dictates chemical composition of interstellar grain mantle. Composition of grain mantle which depends on mobility of H and O atoms are already discussed in Das et al. (2008a); Das et al. (2010) and Das & Chakrabarti (2011). We assume that the gas phase species are physisorbed onto dust grains ($\sim 0.1 \mu\text{m}$) having a grain number density of $1.33 \times 10^{-12} n_H$, where n_H is the concentration of H nuclei in all forms. Due to the unavailability of the binding energies of deuterated species, we assume that it is the same as their hydrogenated counterparts. Binding energies of all surface species are mainly adopted from Hasegawa & Herbst (1993); Allen & Robinson (1977). For some species, we use binding energies from the latest modeling by Garrod et al. (2008) (use $ED_{\text{CH}_3} = 588 \text{ K}$, $ED_{\text{HCO}/\text{DCO}} = 800 \text{ K}$, $ED_{\text{CH}_3\text{O}/\text{CH}_2\text{DO}} = 1250 \text{ K}$, $ED_{\text{CH}_2\text{OH}/\text{CH}_2\text{OD}} = 2254 \text{ K}$ from Garrod et al. 2008). Since the binding energy of CH_3CO was unavailable. By following the binding energy of CH_2CO in Allen & Robinson (1977), we consider the binding energy of CH_3CO to be 2520 K.

To construct the surface reaction network, we primarily follow Hasegawa et al. (1992); Cuppen & Herbst (2007) and Das et al. (2010, 2011, 2014). For the deuterium fractionation reactions on a grain surface, we primarily follow Caselli (2002); Cazau et al. (2010); Garrod et al. (2008) and Das et al. (2014). Formation and destruction pathways of methyl acetate along with its singly deuterated isotopomers and its two isomers are given in Table 2. We also include photo dissociations of

surface species by following Garrod et al. (2008). Photo dissociation of methyl acetate and its deuterated species are included by following Sivaraman et al. (2014). Various evaporation processes are adopted, namely: (a) thermal evaporation, (b) cosmic ray induced evaporation and (c) non-thermal desorption. Due to the lower adsorption energies of the lighter species (H, D, O etc.), thermal evaporation is very efficient. Heavier surface species mostly remain on the grain surface after their formation or accretion from the gas phase. During the late stage of the evolution process, cosmic ray induced evaporation serves as an efficient means to transfer surface species into the gas phase. Another important evaporation mechanism is the non-thermal desorption process. Due to the energy release during some reactions, adsorbed species could be desorbed just after their formation. Garrod et al. (2007) estimated that a fraction ' f ' of the product species in qualifying reactions could desorb immediately and the rest $(1 - f)$ fraction remains as a surface bound product. Here, we apply this mechanism to all surface reactions which result in a single product. Fraction ' f ' is calculated by $f = \frac{aP}{(1+aP)}$, where, a is the ratio between surface molecule bond frequency to frequency at which energy is lost to the grain surface. Here, we choose $a = 0.05$ for all our surface reactions. All these evaporation processes are discussed in detail in our earlier models (Majumdar et al. 2014a; Majumdar et al. 2014b; Das et al. 2015).

TABLE 1
REACTION NETWORK OF VARIOUS FORMS OF METHYL ACETATE AND ITS TWO ISOMERS IN GAS PHASE

$\text{C}_2\text{H}_5\text{D}^+$ + e- → C_2H_3 + D + H + H (D16)	Dissociative Recombination	5.29×10^{-07} cm ³ s ⁻¹
$\text{CH}_3\text{OCH}_3\text{D}^+$ + e- → $\text{CH}_3\text{OCH}_2\text{D}$ + H (D17)	Dissociative Recombination	8.22×10^{-07} cm ³ s ⁻¹
$\text{CH}_3\text{OCH}_2\text{D}^+$ + e- → O + CH_3 + CH_2D (D18)	Dissociative Recombination	8.22×10^{-07} cm ³ s ⁻¹
$\text{CH}_3\text{OCH}_2\text{D}^+$ + e- → CH_3OD + CH_2 (D19)	Dissociative Recombination	8.22×10^{-07} cm ³ s ⁻¹
$\text{HCOOC}_2\text{H}_6^+$ + e- → $\text{C}_2\text{H}_5\text{OCHO}$ + H (D20)	Dissociative Recombination	1.56×10^{-06} cm ³ s ⁻¹
$\text{C}_3\text{H}_7\text{O}_2^+$ + e- → $\text{C}_2\text{H}_5\text{OCHO}$ + H (D21)	Dissociative Recombination	1.56×10^{-06} cm ³ s ⁻¹
$\text{C}_3\text{H}_7\text{O}_2^+$ + e- → $\text{CH}_3\text{COOCH}_3$ + H (D22)	Dissociative Recombination	1.56×10^{-06} cm ³ s ⁻¹
$\text{C}_3\text{H}_7\text{O}_2^+$ + e- → $\text{CH}_3\text{COCH}_2\text{OH}$ + H (D23)	Dissociative Recombination	1.56×10^{-06} cm ³ s ⁻¹
$\text{C}_3\text{H}_6\text{DO}_2^+$ + e- → $\text{C}_2\text{H}_4\text{DOCHO}$ + H (D24)	Dissociative Recombination	1.56×10^{-06} cm ³ s ⁻¹
$\text{CH}_3\text{COOCH}_3$ + CRPHOT → $\text{C}_3\text{H}_6\text{O}_2^+$ + e- (C1)	Cosmic ray induced photoreaction	3.25×10^{-14} s ⁻¹
$\text{C}_2\text{H}_5\text{OCHO}$ + CRPHOT → $\text{C}_3\text{H}_6\text{O}_2^+$ + e- (C2)	Cosmic ray induced photoreaction	3.25×10^{-14} s ⁻¹
$\text{CH}_3\text{COCH}_2\text{OH}$ + CRPHOT → $\text{C}_3\text{H}_6\text{O}_2^+$ + e- (C3)	Cosmic ray induced photoreaction	3.25×10^{-14} s ⁻¹
$\text{CH}_3\text{COOCH}_2\text{D}$ + CRPHOT → $\text{C}_3\text{H}_5\text{DO}_2^+$ + e- (C4)	Cosmic ray induced photoreaction	3.25×10^{-14} s ⁻¹
$\text{CH}_2\text{DCOOCH}_3$ + CRPHOT → $\text{C}_3\text{H}_5\text{DO}_2^+$ + e- (C5)	Cosmic ray induced photoreaction	3.25×10^{-14} s ⁻¹
$\text{CH}_3\text{COOCH}_3$ + CRPHOT → C_2H_6 + CO_2 (C6)	Cosmic ray induced photoreaction	1.63×10^{-14} s ⁻¹
$\text{C}_2\text{H}_5\text{OCHO}$ + CRPHOT → C_2H_6 + CO_2 (C7)	Cosmic ray induced photoreaction	1.63×10^{-14} s ⁻¹
$\text{CH}_3\text{COCH}_2\text{OH}$ + CRPHOT → C_2H_6 + CO_2 (C8)	Cosmic ray induced photoreaction	1.63×10^{-14} s ⁻¹
$\text{CH}_3\text{COOCH}_2\text{D}$ + CRPHOT → $\text{C}_2\text{H}_5\text{D}$ + CO_2 (C9)	Cosmic ray induced photoreaction	1.63×10^{-14} s ⁻¹
$\text{CH}_2\text{DCOOCH}_3$ + CRPHOT → $\text{C}_2\text{H}_5\text{D}$ + CO_2 (C10)	Cosmic ray induced photoreaction	1.63×10^{-14} s ⁻¹
C_2H_6 + CRPHOT → C_2H_6^+ + e- (C11)	Cosmic ray induced photoreaction	1.26×10^{-14} s ⁻¹
$\text{C}_2\text{H}_5\text{D}$ + CRPHOT → $\text{C}_2\text{H}_5\text{D}^+$ + e- (C12)	Cosmic ray induced photoreaction	1.26×10^{-14} s ⁻¹
$\text{C}_2\text{H}_5\text{D}$ + CRPHOT → C_2H_4 + HD (C13)	Cosmic ray induced photoreaction	6.11×10^{-14} s ⁻¹
$\text{C}_2\text{H}_4\text{DOCHO}$ + CRPHOT → $\text{C}_3\text{H}_5\text{DO}_2^+$ + e- (C14)	Cosmic ray induced photoreaction	3.25×10^{-14} s ⁻¹
$\text{C}_2\text{H}_4\text{DOCHO}$ + CRPHOT → $\text{C}_3\text{H}_5\text{D}$ + CO_2 (C15)	Cosmic ray induced photoreaction	3.25×10^{-14} s ⁻¹
$\text{CH}_3\text{COOCH}_3$ + PHOTON → C_2H_6 + CO_2 (P1)	Photoreactions	4.54×10^{-14} s ⁻¹
$\text{C}_2\text{H}_5\text{OCHO}$ + PHOTON → C_2H_6 + CO_2 (P2)	Photoreactions	4.54×10^{-14} s ⁻¹
$\text{CH}_3\text{COOCH}_2\text{D}$ + PHOTON → $\text{C}_2\text{H}_5\text{D}$ + CO_2 (P3)	Photoreactions	4.54×10^{-14} s ⁻¹
$\text{CH}_2\text{DCOOCH}_3$ + PHOTON → $\text{C}_2\text{H}_5\text{D}$ + CO_2 (P4)	Photoreactions	4.54×10^{-14} s ⁻¹
$\text{CH}_3\text{COOCH}_3$ + PHOTON → CH_3OCH_3 + CO (P5)	Photoreactions	4.54×10^{-14} s ⁻¹
$\text{C}_2\text{H}_5\text{OCHO}$ + PHOTON → CH_3OCH_3 + CO (P6)	Photoreactions	4.54×10^{-14} s ⁻¹
$\text{CH}_3\text{COCH}_2\text{OH}$ + PHOTON → CH_3OCH_3 + CO (P7)	Photoreactions	4.54×10^{-14} s ⁻¹
$\text{CH}_3\text{COOCH}_2\text{D}$ + PHOTON → $\text{CH}_3\text{OCH}_2\text{D}$ + CO (P8)	Photoreactions	4.54×10^{-14} s ⁻¹
$\text{CH}_2\text{DCOOCH}_3$ + PHOTON → $\text{CH}_3\text{OCH}_2\text{D}$ + CO (P9)	Photoreactions	4.54×10^{-14} s ⁻¹
$\text{CH}_3\text{COOCH}_3$ + PHOTON → CH_3OH + H_2CCO (P10)	Photoreactions	4.54×10^{-14} s ⁻¹
$\text{C}_2\text{H}_5\text{OCHO}$ + PHOTON → CH_3OH + H_2CCO (P11)	Photoreactions	4.54×10^{-14} s ⁻¹
$\text{CH}_3\text{COCH}_2\text{OH}$ + PHOTON → CH_3OH + H_2CCO (P12)	Photoreactions	4.54×10^{-14} s ⁻¹
$\text{CH}_2\text{DCOOCH}_3$ + PHOTON → CH_2DOH + H_2CCO (P13)	Photoreactions	4.54×10^{-14} s ⁻¹
$\text{CH}_3\text{COOCH}_2\text{D}$ + PHOTON → CH_2DOH + H_2CCO (P14)	Photoreactions	4.54×10^{-14} s ⁻¹
$\text{CH}_3\text{COOCH}_3$ + PHOTON → CH_3O + CH_3CO (P15)	Photoreactions	4.54×10^{-14} s ⁻¹
$\text{C}_2\text{H}_5\text{OCHO}$ + PHOTON → CH_3O + CH_3CO (P16)	Photoreactions	4.54×10^{-14} s ⁻¹
$\text{CH}_3\text{COCH}_2\text{OH}$ + PHOTON → CH_2OH + CH_3CO (P17)	Photoreactions	4.54×10^{-14} s ⁻¹
$\text{CH}_3\text{COCH}_2\text{OH}$ + PHOTON → CH_2OH + CH_3CO (P18)	Photoreactions	4.54×10^{-14} s ⁻¹
$\text{CH}_3\text{COOCH}_2\text{D}$ + PHOTON → CH_2DO + CH_3CO (P19)	Photoreactions	4.54×10^{-14} s ⁻¹
$\text{CH}_2\text{DCOOCH}_3$ + PHOTON → CH_2DO + CH_3CO (P20)	Photoreactions	4.54×10^{-14} s ⁻¹
CH_3CO + PHOTON → CH_3 + CO (P21)	Photoreactions	4.54×10^{-14} s ⁻¹
C_2H_6 + PHOTON → C_2H_6^+ + e- (P22)	Photoreactions	2.78×10^{-21} s ⁻¹
C_2H_6 + PHOTON → C_2H_4 + H_2 (P23)	Photoreactions	4.14×10^{-17} s ⁻¹
$\text{CH}_3\text{OCH}_2\text{D}$ + PHOTON → H_2CO + CH_3D (P24)	Photoreactions	4.72×10^{-20} s ⁻¹
$\text{CH}_3\text{OCH}_2\text{D}$ + PHOTON → $\text{CH}_3\text{OCH}_2\text{D}^+$ + e- (P25)	Photoreactions	4.72×10^{-20} s ⁻¹
$\text{C}_2\text{H}_4\text{DOCHO}$ + PHOTON → $\text{C}_2\text{H}_5\text{D}$ + CO_2 (P26)	Photoreactions	4.54×10^{-14} s ⁻¹
$\text{C}_2\text{H}_4\text{DOCHO}$ + PHOTON → $\text{CH}_3\text{OCH}_2\text{D}$ + CO (P27)	Photoreactions	4.54×10^{-14} s ⁻¹
$\text{C}_2\text{H}_4\text{DOCHO}$ + PHOTON → CH_2DOH + H_2CCO (P28)	Photoreactions	4.54×10^{-14} s ⁻¹
$\text{C}_2\text{H}_4\text{DOCHO}$ + PHOTON → CH_2DO + CH_3CO (P29)	Photoreactions	4.54×10^{-14} s ⁻¹
$\text{C}_2\text{H}_5\text{OCHO}$ + PHOTON → CH_2OH + CH_3CO (P30)	Photoreactions	4.54×10^{-14} s ⁻¹

2.3. Physical condition

Chemical composition of a molecular cloud is heavily dependent on the physical properties of the cloud. Thus it is essential to consider suitable physical condition for astrochemical modeling. Viti et al. (2004); Garrod & Herbst (2006) & Garrod et al. (2008) considered an isothermal ($T = 10$ K) collapsing cloud (collapsing from $n_H = 3 \times 10^3$ cm $^{-3}$ to $n_H = 10^7$ cm $^{-3}$) for their astrochemical modeling. Here also, we consider similar collapsing cloud model and consider that this collapsing process would continue up to 10^6 years. In Fig. 1, we show the time evolution of densities.

Survival of complex molecules in and around any molecular cloud is strongly related to the effect of interstellar radiation field and thus upon the visual extinction (A_V) parameter. Depending on the number density of the cloud, we vary visual extinction parameter by following the relation used in Lee et al. (1996) and Das & Chakrabarti (2011). Relationship between the number density of hydrogen and visual extinction is given by,

$$n_H = n_{H0} [1 + (\sqrt{n_{Hmax}/n_{H0}} - 1) A_V / A_{Vmax}]^2, \quad (8)$$

where, n_{H0} is the cloud density at the cloud surface ($= 3 \times 10^3$ cm $^{-3}$), n_{Hmax} is the maximum density ($= 10^7$ cm $^{-3}$) and A_{Vmax} ($= 150$) is the maximum visual extinction considered very deep inside the cloud. Variation of A_V with respect to n_H is shown in Fig. 1a.

In order to consider more realistic situation, following the consideration of Viti et al. (2004); Garrod & Herbst (2006) and Garrod et al. (2008), here, we use two phase physical model to mimic the evolution of the interstellar condition. First phase is the collapsing phase what we just have discussed above and second phase is the warm up phase. Collapsing phase continues up to 10^6 year and in the warm up phase, it is assumed that the collapse has just stopped and temperature started to rise from 10 K and would reach 200 K. This warm up phase will continue up to another 10^6 years. This is the typical time scale for the low mass star formation (Viti et al. 2004). Fig. 1b shows the time evolution of temperatures during our simulation regime. So in brief, our simulation time scale continues for 2×10^6 years – the collapsing phase takes 10^6 years and the warm up phase takes up another 10^6 years.

2.4. Results of chemical modeling

Here, we consider a molecular gas to begin with. For this, we need to choose initial constituents relevant to a dense cloud. Our adopted initial composition is shown in Table 3. This condition is adopted by following Das et al. (2014) and references therein. As in the case of hydrogen atom, it is assumed that initially all deuteriums are locked in the form of HD. Initial atomic D/H ratio is assumed to be 0.1.

Armed with our physical model (presented in Fig. 1) and chemical model as discussed in Section 2, we show time evolution of the abundances of CH₃COOCH₃, CH₂DCOOCH₃/CH₃COOCH₂D, C₂H₅COOCH₃ and CH₃COCH₂OH in gas phase and ice phase in Fig. 2. Solid curves in Fig. 2 are used to represent the gas phase species and dashed curves are used to represent the ice phase species.

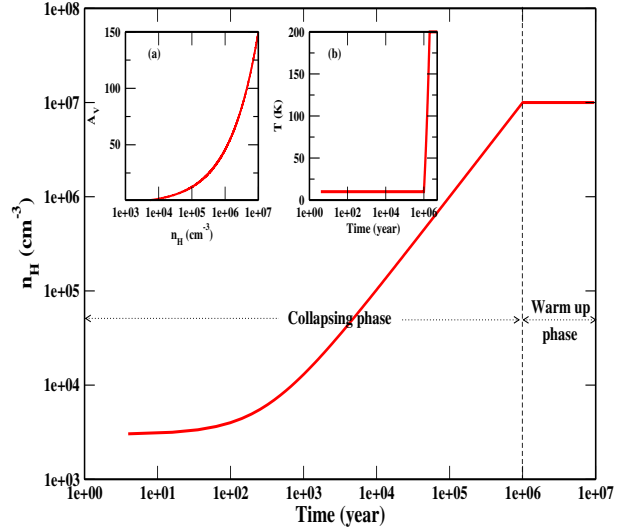


FIG. 1.— Time evolution of densities during collapsing and warm up phase of a cloud. Fig. 1a (inset picture) represent the variation of visual extinction (A_V) with respect to the hydrogen number density (n_H) and Fig. 1b (inset picture) represent the time dependent temperature profile of the cloud.

We are considering two phase model. During the collapsing phase, cloud collapses isothermally ($T = 10$ K). Due to low temperature in the collapsing phase, several species are formed on the ice phase. It is clear from Fig. 2 that methyl acetate and its related species are mainly formed on the ice phase during this collapsing period. In the gas phase, these molecules are produced sufficiently but due to the depletion of gas phase species, their net production is not high. At low temperatures, depleted species are unable to overcome the energy barriers on the grain surfaces and thus mostly remain trapped on the interstellar ices. Under this circumstances, cosmic ray induced desorption and non-thermal desorption mechanisms discussed in the Section 2.2 play a crucial role to transfer some surface species to the gas phase. During the warm up phase, temperature reaches around ~ 100 K and almost all the surface species are transferred to the gas phase. As a result, we see a sudden rise in the gas phase abundance profile at the cost of sharp drop in the ice phase abundance profile. Beyond 100 K, production of surface species is not possible due to the short residence time of the surface species. Thus production would continue only in the gas phase. However, beyond 100 K, gas phase molecules are dissociated by various means. Due to the unavailability of reactants, production of gas phase species is also hampered.

The peak abundance of the gas phase species is obtained at a time when all the surface species are transferred to the gas phase. Peak abundances of gas phase CH₃COOCH₃, CH₂DCOOCH₃/CH₃COOCH₂D, C₂H₅COOCH₃ and CH₃COCH₂OH are found to be 7.17×10^{-10} , 6.10×10^{-11} , 3.50×10^{-12} , 1.82×10^{-12} respectively. For the ice phase species, peak abundances of CH₃COOCH₃, CH₂DCOOCH₃/CH₃COOCH₂D, C₂H₅COOCH₃ and CH₃COCH₂OH are found to be 1.21×10^{-08} , 1.42×10^{-09} , $7.30 \times$

TABLE 2
FORMATION/DESTRUCTION OF VARIOUS FORMS OF METHYL ACETATE AND ITS TWO ISOMERS IN ICE PHASE

Reaction	Rate coefficients at 10 K(sec ⁻¹)
CH ₃ + CO → CH ₃ CO	7.91 × 10 ⁻⁰³
CH ₃ O + CH ₃ CO → CH ₃ COOCH ₃	2.31 × 10 ⁻¹⁰
CH ₂ DO + CH ₃ CO → CH ₂ DCOOCH ₃	2.30 × 10 ⁻¹⁰
CH ₂ OH + CH ₃ → C ₂ H ₅ OH	7.91 × 10 ⁻⁰³
H + C ₂ H ₅ O → C ₂ H ₅ OH	4.91 × 10 ⁺⁰¹
HCO + C ₂ H ₅ O → C ₂ H ₅ OCHO	1.14 × 10 ⁻⁰⁵
H + CH ₂ OCHO → CH ₃ OCHO	4.91 × 10 ⁺⁰¹
CH ₃ + CH ₂ OCHO → C ₂ H ₅ OCHO	7.91 × 10 ⁻⁰³
HCO + CH ₃ O → CH ₃ OCHO	1.15 × 10 ⁻⁰⁵
CH ₂ OH + CH ₃ CO → CH ₃ COCH ₂ OH	2.12 × 10 ⁻¹⁰
C ₂ H ₅ OH + CRPHOT → C ₂ H ₅ O + H	1.30 × 10 ⁻¹⁷
C ₂ H ₅ OCHO + CRPHOT → CH ₂ OCHO + CH ₃	1.30 × 10 ⁻¹⁷
C ₂ H ₅ OCHO + CRPHOT → C ₂ H ₅ O + HCO	1.30 × 10 ⁻¹⁷
CH ₃ OCHO + CRPHOT → CH ₂ OCHO + H	1.30 × 10 ⁻¹⁷
CH ₃ COOCH ₃ + CRPHOT → C ₂ H ₆ + CO ₂	1.30 × 10 ⁻¹⁷
C ₂ H ₅ OCHO + CRPHOT → C ₂ H ₆ + CO ₂	1.30 × 10 ⁻¹⁷
CH ₃ COOCH ₂ D + CRPHOT → C ₂ H ₅ D + CO ₂	1.30 × 10 ⁻¹⁷
CH ₂ DCOOCH ₃ + CRPHOT → C ₂ H ₅ D + CO ₂	1.30 × 10 ⁻¹⁷
CH ₃ COCH ₂ OH + CRPHOT → C ₂ H ₅ D + CO ₂	1.30 × 10 ⁻¹⁷

TABLE 3
INITIAL ABUNDANCES USED RELATIVE TO TOTAL HYDROGEN NUCLEI.

Species	Abundance
H ₂	5.00 × 10 ⁻⁰¹
He	1.00 × 10 ⁻⁰¹
N	2.14 × 10 ⁻⁰⁵
O	1.76 × 10 ⁻⁰⁴
H ₃ ⁺	1.00 × 10 ⁻¹¹
C ⁺	7.30 × 10 ⁻⁰⁵
S ⁺	8.00 × 10 ⁻⁰⁸
Si ⁺	8.00 × 10 ⁻⁰⁹
Fe ⁺	3.00 × 10 ⁻⁰⁹
Na ⁺	2.00 × 10 ⁻⁰⁹
Mg ⁺	7.00 × 10 ⁻⁰⁹
P ⁺	3.00 × 10 ⁻⁰⁹
Cl ⁺	4.00 × 10 ⁻⁰⁹
e ⁻	7.31 × 10 ⁻⁰⁵
HD	1.6 × 10 ⁻⁰⁵

10⁻¹¹, 4.18 × 10⁻¹¹ respectively. Final abundances (i.e., after 2 × 10⁶ years) of gas phase CH₃COOCH₃, CH₂DCOOCH₃/CH₃COOCH₂D, C₂H₅COOCH₃ and CH₃COCH₂OH are found to be 1.07 × 10⁻¹⁸, 2.17 × 10⁻²⁵, 1.64 × 10⁻¹⁴, 1.08 × 10⁻¹⁸ respectively.

Column densities of these species could be calculated by using the following relation used by Shalabiea & Greenberg (1994) and Das et al. (2011,2013a):

$$N(A) = n_H x_i R, \quad (9)$$

where, n_H is the total hydrogen number density, x_i is the abundance of i^{th} species and R is the path length along the line of sight ($= 1.6 \times 10^{21} A_V / n_H$). For the simplicity, we use $A_V = A_{Vmax} = 150$ for the computation. In Table 4, we show column density (peak value obtained in our simulation regime) of these species in gas/ice phase along with some observational results. From Table 4, it is interesting to note that despite a low initial elemental abundance of deuterium ($\sim 10^{-5}$, Linsky et al. 1995) in the interstellar space, singly deuterated isotopomers of methyl acetate are efficiently producing in the ISM.

3. SPECTROSCOPICAL MODELING AND STRUCTURAL CALCULATIONS

Past studies reveal that quantum chemical calculations might serve as important diagnostics for the identification of various species in the ISM. For the computation of rotational transitions, rotational constants are essential. Huang & Lee (2008) showed that their calculated values often lead to the accuracy within 20 MHz for the B and C type constants. There are also several instances where calculated vibrational frequencies are accurate to within 5 cm⁻¹ or even better (Huang & Lee 2008; Huang & Lee 2009; Huang & Lee 2011; Inostroza et al. 2011; Fortenberry & Crawford 2011a; Fortenberry & Crawford 2011b; Fortenberry et al. 2012a; Fortenberry et al. 2012b). Following this type of earlier works, we decided to carry out quantum chemical calculations to find out spectral properties of various forms of methyl acetate. All our spectroscopic calculations do not depend on nuclear spins. This is because ortho and para states of a species differ in the arrangement of the nuclear spins and only in cases of NMR shielding and spin-spin coupling calculation nuclear spin is used in Gaussian 09W program. Other than that, all other properties (energies, geometries, IR, UV-Vis, etc.) computed by Gaussian 09W program are nuclear spin independent

TABLE 4
COLUMN DENSITY OF VARIOUS FORMS OF METHYL ACETATE AND ITS TWO ISOMERS.

Species	Calculated column density (ice phase peak value) (in cm^{-2})	Calculated column density (gas phase peak value) (in cm^{-2})	Calculated Column density (gas phase final value) (in cm^{-2})	Column density (observation/prediction in gas phase) (in cm^{-2})
$\text{CH}_3\text{COOCH}_3$	2.91×10^{15}	1.72×10^{14}	2.58×10^5	$(4.2 \pm 0.5) \times 10^{15}^a$
$\text{CH}_2\text{DCOOCH}_3/\text{CH}_3\text{COOCH}_2\text{D}$	3.41×10^{14}	1.46×10^{13}	5.20×10^{-2}	-
$\text{C}_2\text{H}_5\text{OCHO}$	1.75×10^{13}	8.40×10^{11}	3.95×10^9	$(4.5 \pm 1) \times 10^{14}^a, 5.4 \times 10^{16}^b$
$\text{CH}_2\text{COCH}_2\text{OH}$	1.00×10^{13}	4.38×10^{11}	2.59×10^5	$5.00 \times 10^{12}^c$

^a Tercero et al. (2013) (in Orion)

^b Belloche et al. (2009) (in Sgr B2(N))

^c Apponi et al. (2006) (in Sgr B2(N))

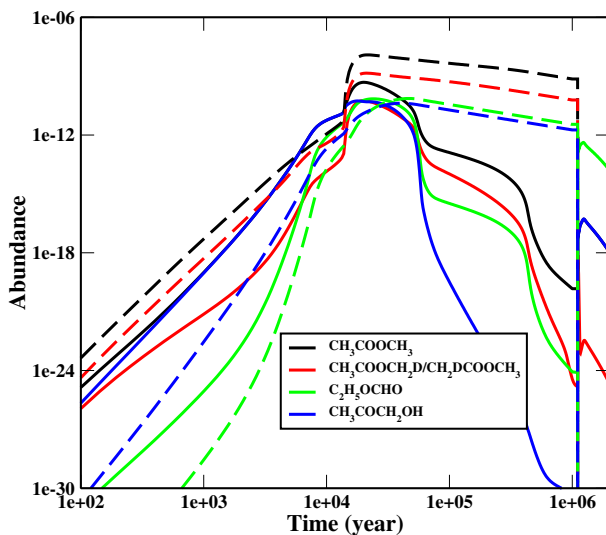


FIG. 2.— Chemical evolution of methyl acetate and some of its related species. Solid curves represents the gas phase species and dashed curves are used to represent the ice phase species.

(as nuclear spin does not appear in the Hamiltonian and thus will not change the optimization or frequencies). Thus, the values would be identical for different ortho and para states and they will be treated as degenerate states for most purposes.

Methyl acetate ($\text{CH}_3\text{COOCH}_3$) is an asymmetric top with C_1 symmetry. Gaussian 09W program is used for the computation of various spectral parameters. B3LYP (Becke 1993; Lee et al. 1988) functional along with the 6-311G++(d,p) basis set is used for the computation of structural parameters as well as ground state energies. Ground state energies of $\text{CH}_3\text{COOCH}_3$ in gas and ice phases (pure water) are found to be -268.4748 *a.u* and -268.4743 *a.u.* respectively. These are identical for its deuterated species without zero-point energy corrections at 0 K. The zero point corrections are crucial for the chemistry of the deuterated species. Our computed zero point vibrational energies for reactants and products of reaction *R1* along with their deuterated counterpart is shown in Table 5.

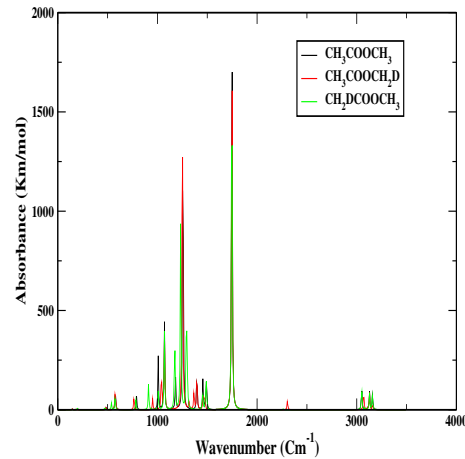


FIG. 3.— Infrared spectra of ice phase $\text{CH}_3\text{COOCH}_3$, $\text{CH}_2\text{DCOOCH}_3$, $\text{CH}_3\text{COOCH}_2\text{D}$.

3.1. Vibrational spectroscopy

Here also, we use B3LYP functional with 6-311++G(d,p) basis set for the computation of the gas phase vibrational transitions of various forms of methyl acetate. For the ice phase vibrational transitions, Polarizable Continuum Model (PCM) with the integral equation formalism variant (IEFPCM) as a default Self-consistent Reaction Field (SCRF) method are used.

In Table 6, we present vibrational frequencies of $\text{CH}_3\text{COOCH}_3$ and two of its isotopomers ($\text{CH}_2\text{DCOOCH}_3$ and $\text{CH}_3\text{COOCH}_2\text{D}$). For gas phase $\text{CH}_3\text{COOCH}_3$, the strongest peak appears at 1261.28 cm^{-1} . In case of ice phase, it is noted that this peak appears at 1256.02 cm^{-1} . Next strongest gas phase peak appears at 1796.16 cm^{-1} which is shifted in the ice phase. In case of various isotopes of methyl acetate, we have different transitions. These differences are attributed to the changes of masses of isotopes. Each of $\text{CH}_3\text{COOCH}_3$, $\text{CH}_2\text{DCOOCH}_3$ and $\text{CH}_3\text{COOCH}_2\text{D}$ has a different spectrum. We find that the most intense mode of $\text{CH}_2\text{DCOOCH}_3$ in the gas phase appears at 1795.20 cm^{-1} . This peak is shifted in the ice phase by nearly 50 cm^{-1} , i.e., at 1746.56 cm^{-1} . The second strongest peak in the gas phase which appears at 1238.04 cm^{-1} is also shifted in the ice phase and appears at 1233.76 cm^{-1} . In Fig. 3, we show how the isotopic substitution ($\text{CH}_2\text{DCOOCH}_3$, $\text{CH}_3\text{COOCH}_2\text{D}$) plays a part in vibrational transitions of $\text{CH}_3\text{COOCH}_3$ in ice phase. Table 6 clearly shows the differences between

TABLE 5
COMPUTED ZERO-POINT VIBRATIONAL ENERGIES

Species	Zero-point vibrational energy (in gas phase) (in KJ/Mol)	Zero-point vibrational energy (in ice phase) (in KJ/Mol)
CH ₃ CO	112.845869	112.65102
CH ₃ O	97.2549462	97.0678377
CH ₂ DCO	104.789033	104.608828
CH ₂ DO	88.6389605	88.4619354
CH ₃ COOCH ₃	234.334167	233.7121732
CH ₃ COOCH ₂ D	225.736088	225.094221
CH ₂ DCOOCH ₃	226.205868	225.540403

spectroscopic parameters computed for interstellar methyl acetate in gas phase and in ice phase. Moreover, in Table 6, we show band assignments and compare our results with the existing theoretical and experimental (Sivaraman et al. 2013; George et al. 1974) results (Senent et al. 2013). Our results are in good agreement with experimental results on solid phase methyl acetate (Sivaraman et al. 2013). Any discrepancy could be attributed to two reasons. First, the experiment was performed at 15 K, while we calculate vibrational transitions by ab-initio method (i.e., at 0 K). Second, in our quantum chemical simulation, we consider a single methyl acetate inside a spherical cavity while in the experiment, deposited numbers of methyl acetate could form clusters. In order to determine column density (by using Lambert-Beer relationship used in Bennett et al., 2004) of methyl acetate, it is required to find out integrated numerous absorption features. To know the integrated absorption features, corresponding integral absorption coefficients ('A' values in units of cm molecule⁻¹) have to be calculated. In Table 6, we show our calculated integral absorption coefficients for those transitions, which were present in (Sivaraman et al. 2013). These values could be used to predict the column densities of the experimental methyl acetate ice.

TABLE 6

VIBRATIONAL FREQUENCIES OF VARIOUS FORMS OF METHYL ACETATE IN GAS PHASE, IN WATER ICE AT B3LYP/6-311G++(D,P) LEVEL OF THEORY

Species	Peak positions (Gas phase) (in cm ⁻¹)	Absorbance (in km/mol)	Peak positions (H ₂ O ice) (in cm ⁻¹)	Absorbance (in km/mol)/ Integral absorption coefficient for experimentally obtained transitions (in cm molecule ⁻¹)	Band assignments	Experimental/ calculated values (in cm ⁻¹)
$\text{CH}_3\text{COOCH}_3$	47.27	0.2090	54.65	0.0002	CH_3 torsion	43 ^c
	130.25	0.644	146.91	1.078	CH_3 torsion	154 ^c
	181.78	7.76	200.71	1.421	torsion	203 ^a , 182 ^c
	280.99	13.083	312.14	0.076	COC bending	302 ^a , 291 ^c
	424.03	5.595	487.62	3.774	CCO bending	433 ^a , 426 ^c
	610.49	5.636	575.95	20.921	$\text{C}=\text{O}$ wagging	609 ^a , 611 ^c
	643.41	5.057	580.98	11.338	skeletal deformation	638 ^a , 651 ^c
	855.46	23.369	791.11	19.998 / 3.32 × 10 ⁻¹⁸	skeletal deformation	846 ^a , 849 ^b , 869 ^c
	983.30	1.773	1008.14	78.214 / 1.29 × 10 ⁻¹⁷	CH_3 rocking	982 ^a , 977 ^b , 999 ^c
	1066.92	6.90	1058.74	14.958	CH_3 rocking	1073 ^c
	1068.53	83.157	1070.45	128.917 / 2.14 × 10 ⁻¹⁷	$\text{O}-\text{CH}_3$ stretching	1051 ^a , 1044 ^b , 1096 ^c
	1171.58	0.897	1160.62	1.186 / 1.96 × 10 ⁻¹⁹	CH_3 rocking	1161 ^a , 1191.7 ^b , 1192 ^c
	1206.93	0.737	1181.41	53.014	CH_3 rocking	1190 ^a , 1219 ^c
	1261.28	349.202	1256.02	499.628 / 8.29 × 10 ⁻¹⁷	skeletal deformation	1249 ^a , 1246.2 ^b , 1291 ^c
	1399.64	44.351	1396.14	63.908 / 1.06 × 10 ⁻¹⁷	CH_3 bending	1372 ^a , 1368.7 ^b , 1406 ^c
	1469.96	12.398	1456.57	44.4885 / 7.38 × 10 ⁻¹⁸	CH_3 bending	1438 ^a , 1439.5 ^b , 1484 ^c
	1473.17	20.3577	1468.48	4.806 / 7.97 × 10 ⁻¹⁹	CH_3 bending	1438 ^a , 1464.5 ^b , 1490 ^c
	1477.55	8.18	1477.07	0.8812	CH_3 bending	1445 ^a , 1496 ^c
	1483.88	10.634	1489.38	26.002	CH_3 bending	1462 ^a , 1506 ^c
	1498.32	9.488	1494.58	31.576	CH_3 bending	1455 ^a , 1521 ^c
	1796.16	288.670	1747.67	659.267 / 1.09 × 10 ⁻¹⁶	$\text{C}=\text{O}$ stretching	1747 ^a , 1735.7 ^b , 1809 ^c
	3050.07	6.1048	3048.63	21.887 / 3.63 × 10 ⁻¹⁸	CH_3 stretching	2955 ^a , 2997.7 ^b , 3097 ^c
	3051.09	16.3520	3052.37	14.406 / 2.39 × 10 ⁻¹⁸	CH_3 stretching	2940 ^a , 3021.5 ^b , 3102 ^c
	3110.74	5.393	3110.28	2.562	CH_3 stretching	3002 ^a , 3186 ^c
	3122.45	20.665	3127.81	28.399	CH_3 stretching	3002 ^a , 3189 ^c
	3155.83	9.417	3158.73	23.852	CH_3 stretching	3028 ^a , 3222 ^c
	3156.53	11.217	3160.55	1.808	CH_3 stretching	3028 ^a , 3225 ^c
$\text{CH}_2\text{DCOOCH}_3$	41.04	0.067	51.68	0.0911	CH_3 torsion	
	130.06	0.690	140.99	0.560	CH_3 torsion	
	179.61	7.740	194.88	2.040	torsion	
	277.79	12.446	306.38	0.124	COC bending	
	411.93	5.797	473.08	3.566	CCO bending	
	565.46	5.322	538.17	10.404	$\text{C}=\text{O}$ wagging	
	639.25	5.150	575.97	19.820	skeletal deformation	
	853.19	23.930	783.20	14.752	skeletal deformation	
	898.09	2.462	911.30	41.344	CH_3 rocking	
	1007.10	5.250	1008.63	27.630	CH_3 rocking	
	1056.67	65.689	1070.05	120.315	$\text{O}-\text{CH}_3$ stretching	
	1171.58	0.8675	1160.61	1.257	CH_3 rocking	
	1206.05	1.783	1173.46	118.272	CH_3 rocking	
	1238.04	260.244	1233.76	321.961	skeletal deformation	
	1302.53	79.1404	1291.62	185.405	CH_3 bending	
	1311.42	76.069	1302.97	26.988	CH_3 bending	
	1458.38	11.527	1453.26	30.510	CH_3 bending	
	1470.87	15.677	1477.05	0.944	CH_3 bending	
	1483.85	9.590	1487.44	34.191	CH_3 bending	
	1498.32	9.599	1492.18	24.069	CH_3 bending	
	1795.20	293.616	1746.56	670.696	$\text{C}=\text{O}$ stretching	
	2263.50	1.683	2262.84	1.310	CH_3 stretching	
	3050.34	29.712	3049.58	35.303	CH_3 stretching	
	3078.54	4.062	3079.32	2.277	CH_3 stretching	
	3122.45	20.575	3127.68	26.847	CH_3 stretching	
	3151.52	5.663	3155.56	11.459	CH_3 stretching	
	3155.87	14.781	3159.20	13.631	CH_3 stretching	

^a George et al. (1974) (gas phase experiment)

^b Sivaraman et al. (2014) (ice phase experiment)

^c Senent et al. (2013) (theoretical calculations for gas phase by using MP2/cc-pVTZ level of theory)

Species	Peak positions (Gas phase) (in cm^{-1})	Absorbance (in km/mol)	Peak positions (H_2O ice) (in cm^{-1})	Absorbance (in km/mol)/ Integral absorption coefficient for experimentally obtained transitions (in cm molecule^{-1})	Band assignments	Experimental/ calculated values (in cm^{-1})
$\text{CH}_3\text{COOCH}_2\text{D}$	47.24	0.220	49.46	0.0009	CH_3 torsion	
	117.08	6.318	146.14	1.146	CH_3 torsion	
	176.79	7.851	182.51	0.752	torsion	
	272.21	12.529	302.79	0.060	COC bending	
	422.11	5.523	482.41	3.599	CCO bending	
	610.20	5.577	573.70	19.981	C=O wagging	
	640.91	5.248	580.96	11.367	skeletal deformation	
	795.99	13.020	765.54	22.042	skeletal deformation	
	981.34	3.634	952.12	16.029	CH_3 rocking	
	1033.62	10.259	1039.70	63.2145	CH_3 rocking	
	1066.63	6.914	1058.65	15.014	$O - \text{CH}_3$ stretching	
	1068.93	80.445	1011.82	113.975	CH_3 rocking	
	1119.12	0.121	1111.58	0.0899	CH_3 rocking	
	1260.55	339.071	1250.04	570.059	$O - \text{CH}_3$ stretching	
	1320.11	6.727	1317.61	11.506	CH_3 rocking	
	1361.98	13.000	1367.32	30.669	CH_3 rocking	
	1401.89	60.743	1396.14	62.187	CH_3 bending	
	1472.26	16.343	1459.23	30.448	CH_3 bending	
	1477.58	9.424	1473.12	19.729	CH_3 bending	
	1495.16	7.333	1480.91	5.211	CH_3 bending	
	1795.00	288.676	1747.40	661.5813	C=O stretching	
	2299.03	16.867	2304.94	14.794	CH_3 stretching	
	3050.81	2.367	3051.19	0.099	CH_3 stretching	
	3074.13	20.519	3069.56	30.683	CH_3 stretching	
	3110.73	5.394	3110.27	2.541	CH_3 stretching	
	3122.22	20.407	3127.54	28.001	CH_3 stretching	
	3156.50	6.463	3160.18	8.432	CH_3 stretching	

3.2. Rotational spectroscopy

Density functional theory (DFT) along with some suitable basis sets are known to accurately calculate spectral properties of various interstellar molecules (Runge & Gross 1984; Puletti et al. 2010; Pieve et al. 2014). Accuracy of computed rotational frequencies depends on the choices of the models. Recently, Carles et al. (2013, 2014) explained experimental rotational frequencies of 4-methylcyanoallene and ethyl cyanoacetylene with high-level quantum chemical calculations at the B3LYP/cc-pVTZ level of theory by using Gaussian 09W program. Their results are in excellent agreement with the experiment. By following their procedure, we similarly use Beckes three parameter hybrid functional (Becke 1988) employing the Lee, Yang, and Parr correlation functional (B3LYP; Lee et al., 1988) in DFT to calculate rotational constants and Watsons S-reduction quartic and sextic centrifugal distortion constants (Watson 1977) observing the precautions of McKean et al. (2008). But there are also few other studies where CCSD level of theory have been used for the computation of rotational and distortional constants (Fortenberry et al. 2012a; Fortenberry et al. 2012b; Fortenberry et al. 2013). Computation of the anharmonic frequencies require the use of analytic second derivative of energies at the displaced geometries. But the CCSD method in Gaussian 09W program only implements energies. Thus, analytical second derivative of energies are not available at this level of theory. In fact, there are no options in Gaussian 09W program to compute rotational and distortional constants at the CCSD level of theory. This prompted us to use B3LYP functional along with the Peterson and Dunnings correlation consistent (cc-pVTZ) basis set (Peterson & Dunning 2002; Carles et al. 2013) which are proven to yield satisfactory results (Carles et al. 2013; Carles et al. 2014; Das et al. 2015) and also takes less CPU time than other highly correlated methods. Many molecules have been detected in interstellar space with internal rotations (Nguyen et al. 2014). Most of these detection were based on the intense laboratory and theoretical work followed by observations with the help of radio telescopes. One of the simplest example of such observation is detection of methanol in Orion A by Lovas et al., (1976). So as like the methanol which includes one methyl top, internal rotation is also important for methyl acetate molecule having two methyl top. Nguyen et al., (2014) mentioned that the main problem of analyzing the rotational spectrum of methyl acetate is the internal rotation of two inequivalent methyl groups with one low ($102.413(20) \text{ cm}^{-1}$) and one intermediate barrier ($424.580(56) \text{ cm}^{-1}$). They predicted lines up to $J = 30$ using BELGI-Cs-2tops code and by considering ground state parameters from Tudoire et al., (2011). However in the experiment of Tudoire et al., (2011), laboratory measurements were limited to $J = 19$ which includes some uncertainty in the predicted lines of Nguyen et al., (2014). In this paper, we have tried to extend the line list till $J = 41$ by computing many J, K dependent parameters as well as the sextic centrifugal distortion constants which was not derived in the experiment of Tudoire et al., (2011). Our computed parameters

considers various symmetries that arise from the interaction of overall rotation and the internal rotations of two methyl tops as well as the interaction of the methyl tops with each other. We have followed the same technique to extend the line list for two isotopomers of $\text{CH}_3\text{COOCH}_3$.

Computed rotational and vibrational interaction parameters are shown in Table 7. Using these rotational and distortional constants, we calculate various rotational transitions for $\text{CH}_3\text{COOCH}_2\text{D}$ and $\text{CH}_2\text{DCOOCH}_3$ in JPL format (Table 8 and Table 9 respectively) by using the ‘SPCAT’ program (Pickett et al. 1991). These catalog files could be used for the detection of the singly deuterated isotopomers of methyl acetate in the ISM.

Das et al. (2015) already discussed the importance of theoretical calculations prior to any astronomical survey. Our computed frequencies, abundances, column densities for various forms of methyl acetate could be used for radiative transfer modeling. These informations would be crucial for observing any species in the ISM (Coutens et al. 2014 and references therein). CASSIS software (an interactive spectrum analyzer, <http://cassis.cesr.fr>) would be appropriate for modeling observations from this type of molecules. Since ethyl formate and hydroxy acetone were already observed, they were already enlisted within CASSIS. Thus we carry out Local Thermodynamic Equilibrium (LTE) modeling for ethyl formate and hydroxy acetone by using CASSIS software. Fig. 4a and Fig. 4b shows emission spectra of ethyl formate and hydroxyacetone respectively. We model this spectrum by using CASSIS software in LTE (assuming the transitions are optically thin). For this modeling, we use source size = 3", excitation temperature (T_{ex}) = 100 K (typical hot core condition), line width (FWHM) = 7 km s^{-1} , $V_{lsr} = 64 \text{ km s}^{-1}$, column density of Ethyl formate = $5.4 \times 10^{16} \text{ cm}^{-2}$ (column density of hydroxyacetone = $5.4 \times 10^{16} \text{ cm}^{-2}$), column density of $H_2 = 1.8 \times 10^{25} \text{ cm}^{-2}$. These parameters are used by following the best fit LTE model of ethyl formate from Belloche et al. (2009). Similar type of modeling would be possible if one use our catalog files (Table 8 and Table 9) under CASSIS software. Because at present it is not possible to include our catalog files directly into CASSIS, in Fig. 5, stick diagram for the rotational transitions of methyl acetate is shown by using ASCP program (Kisiel et al. 1998; Kisiel et al. 2000). Here, we use the catalog file generated by the SPCAT program as an input of ASCP program. Since the partition function in SPACT program is calculated at $T = 300 \text{ K}$, Fig. 5 represents the stick diagram at $T = 300 \text{ K}$.

4. CONCLUSIONS

- Followings are the major results of this paper:
- A complete reaction network is presented to include the formation and destruction of methyl acetate along with its two singly deuterated isotopomers and two isomers of methyl acetate (ethyl formate and hydroxyacetone). Rate coefficients are also calculated indigenously in the absence of any available educated estimations.
 - In order to mimic realistic interstellar features, we use two phase model for the physical properties of the cloud. In the first phase, the cloud is collapsing and in

TABLE 7

THEORETICAL ROTATIONAL PARAMETERS OF METHYL ACETATE AND ITS TWO ISOTOPOMERS AT B3LYP/AUG-CC-PVTZ LEVEL OF THEORY

Species	Rotational constants	Values in MHz	Distortional constants	Values in MHz
$\text{CH}_3\text{COOCH}_3$ in gas phase	A	10251.95	D_J	0.758×10^{-3}
	B	4154.13	D_{JK}	0.440×10^{-2}
	C	3068.82	D_K	0.543×10^{-2}
			d_1	-0.186×10^{-3}
			d_2	0.202×10^{-4}
$\text{CH}_2\text{DCOOCH}_3$ in gas phase	A	9801.87	D_J	0.964×10^{-3}
	B	4017.75	D_{JK}	0.316×10^{-2}
	C	2979.14	D_K	0.727×10^{-2}
			d_1	-0.249×10^{-3}
			d_2	0.683×10^{-4}
$\text{CH}_3\text{COOCH}_2\text{D}$ in gas phase	A	10090.54	D_J	0.649×10^{-3}
	B	3935.64	D_{JK}	0.419×10^{-2}
	C	2934.42	D_K	0.611×10^{-2}
			d_1	-0.155×10^{-3}
			d_2	0.144×10^{-4}

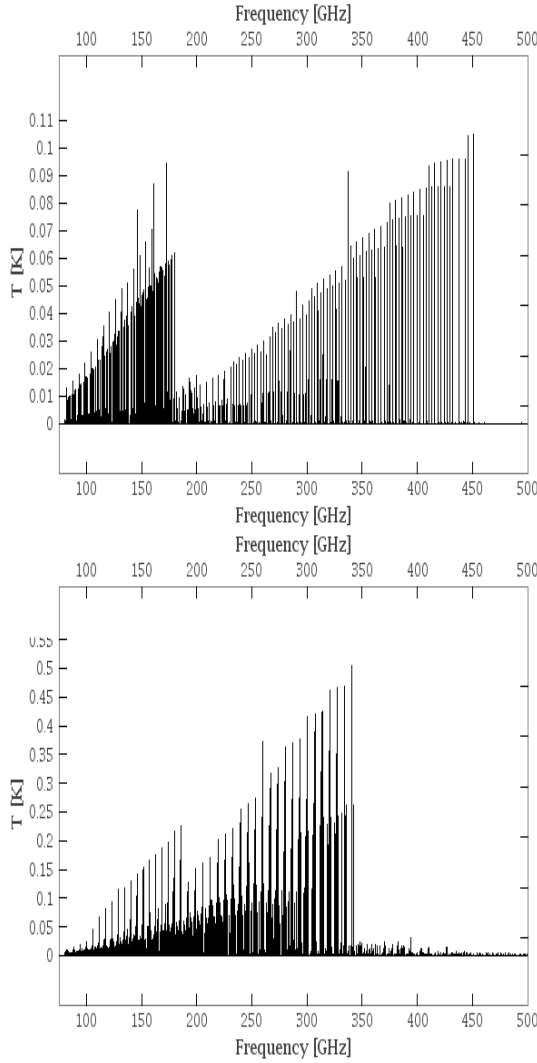


FIG. 4.— LTE model of (a) Ethyl formate and (b) hydroxyacetone.

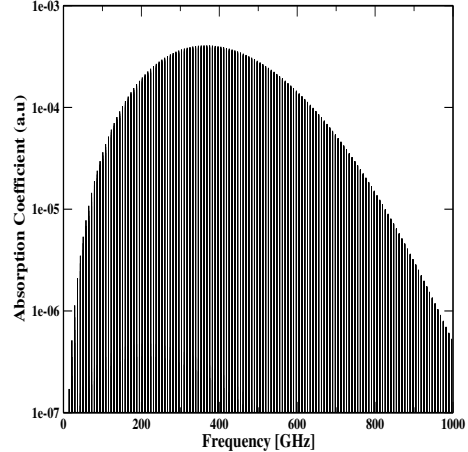


FIG. 5.— Stick diagram of methyl acetate at T=300K

the second phase, the cloud is warming up. We couple our chemical model with this dynamic physical condition and found that methyl acetate along with its two singly deuterated isotopomers could be efficiently formed in gas/ice phase.

- Vibrational and rotational transitions of the various forms of methyl acetate are explored. Our vibrational transitions are compared with the existing experimental/theoretical results and it is found that our results are in good agreement with the experimental results. Based on our calculations of the rotational and distortional constants, we prepare two catalog files for the singly deuterated methyl acetates, which could be useful for its future detection around the region, where methyl acetate has already been observed.

5. ACKNOWLEDGMENTS

AD, PG, DS & SKC are grateful to ISRO respond (Grant No. ISRO/RES/2/372/11-12) and DST (Grant No. SB/S2/HEP-021/2013) for partial financial support. LM thanks MOES and ERC starting grant (3DICE, grant agreement 336474) for funding during this work. Authors also wish to thank Mr. Soumyadip Mondal

(RKMRC, Narendrapur) for his help in data reduction during his M.Sc project work at Indian Centre for Space Physics. We would like to thank the anonymous referee whose valuable suggestions were extremely helpful for improving the content of our paper.

REFERENCES

- Albertsson, T., Semenov, D. A., Vasyunin, A. I., Henning T., Herbst, E., 2013, APJS, 207, 27
- Allen, M., Robinson, G. W., 1977, ApJ, 212, 396
- Apponi, A.J., Hoy, J. J., Halfen, D. T., Ziurys, L. M., 2006, ApJ, 652, 1787
- Blagojevic, V., Petrie, S., & Bohme, D. K., 2003, MNRAS, 339, L7
- Bass, L. M., Kemper, P. R., Anicich, V. G., Bowers, M. T., 1981, J. Am. Chem. Soc., 103, 5283
- Bates, D. R. 1983, ApJ, 270, 564
- Bonnor, W. B., 1956, MNRAS, 116, 351
- Belloche, A., Garrod, R. T., Müller, H. S. P., Menten, K. M., Comito, C., & Schilke, P., 2009, A&A, 499, 215
- Becke, A. D. 1988, Phys. Rev. A, 38, 3098
- Becke A. D., 1993, J. Chem. Phys., 98, 5648
- Bettens, R. P. A., Lee, H. H., Herbst, E., 1995, ApJ, 443, 664
- Bennett, C.J., Jamieson, C., Mebelb, A.M., and Kaiser, R. I., 2004, PCCP, 6, 735
- Carles, S., Mollendal, H., and Guillemin, J.-C., 2013, A&A, 558, A6
- Carles, S., Mollendal, H., Trolez, Y., Guillemin, J., C, 2014, A&A, 564, 82
- Caselli, P., Stantcheva, T., Shalabiea, O., Shematovich, V. I. & Herbst, E., 2002, P&SS, 50, 1257
- Cazaux, S., Cobut, V., Marseille, M., Spaans, M., Caselli, P., 2010, A&A, 522, 74
- Chakrabarti, S., Chakrabarti, S.K., 2000a, A&A 354, L6
- Chakrabarti, S. K., Chakrabarti, S., 2000b, Ind. J. Phys 74B, 97
- Chakrabarti, S.K., 2012, in Proceedings of 'Chemical Evolution of Star Forming Region and Origin of Life', S.K. Chakrabarti, K. Acharyya & A. Das (Eds.), AIP publications No. 1543, (New York, 2013)
- Chakrabarti, S.K., Das, A., Acharyya, K., Chakrabarti, S., 2006, A&A, 457, 167
- Chakrabarti, S.K., Das, A., Acharyya, K., Chakrabarti, S., 2006, BASI, 34, 299
- Chakrabarti, S.K., 2012, AIPC, 1543, 3
- Chakrabarti, S.K., Majumdar, S. K., Das, A. Chakrabarti, S., 2015, Astrophys. Space Sci., DOI: 10.1007/s10509-015-2239-1
- Charnley, S. B., Kress, M. E., Tielens, A. G. G. M., & Millar, T. J., 1995, ApJ, 448, 232
- Clary, D. C., Haider, N., Husain, D., Kabir, M., 1994, ApJ, 422, 416
- Coutens, A. et al., 2014, MNRAS, 445, 1299
- Cuppen, H. M., Herbst, E., 2007, APJ, 668, 294
- Das, A., Chakrabarti, S. K., Acharyya K. & Chakrabarti, S., 2008a, NEWA, 13, 457
- Das, A., Acharyya, K., Chakrabarti, S. & Chakrabarti, S., 2008b, A&A, 486, 209
- Das, A., Acharyya, K. & Chakrabarti, S. K., 2010, MNRAS 409, 789
- Das, A. & Chakrabarti, S. K., 2011, 418, 545, MNRAS
- Das, A., Majumdar, L., Chakrabarti, S. K., & Chakrabarti S., 2013a, NEWA, 23, 118
- Das, A., Majumdar, L., Chakrabarti, S. K., & Saha, R., Chakrabarti, S., 2013b, MNRAS, 433, 3152
- Das, A., Majumdar, L., Chakrabarti, S. K., & Sahu, D., 2015, NEWA, 35, 53
- Delsemme, A.H., 1981, In comets and Origins of Life, Ed. C. Ponnamperuma, 141 (Dordrecht: Reidel)
- Ebert, R., 1955, ZAp, 37, 217
- Federman, S. R., Cardell, J. A., van Dishoeck, E. F., Lambert, D. L., & Black, J. H. 1995, ApJ, 445, 325
- Federman, S. R., Weber, J., & Lambert, D. L. 1996, ApJ, 463, 181
- Foresman, J.B., Frisch, A., 1995-96, Exploring Chemistry with Electronic structure, Gaussian, Inc., Pittsburgh, PA, 15106 USA
- Fortenberry, R. C., & Crawford, T. D. 2011a, J. Chem. Phys., 134, 154304
- Fortenberry, R. C., & Crawford, T. D. 2011b, Annu. Rep. Comput. Chem., 7, 195
- Fortenberry, R. C., & Crawford, T. D. 2011c, JPCA, 115, 8119
- Fortenberry, R. C., Huang, X., Francisco, J. S., Crawford, T. D., & Lee, T. J. 2012a, J. Phys. Chem. A, 116, 9582
- Fortenberry, R. C., Huang, X., Francisco, J. S., Crawford, T. D., & Lee, T. J. 2012b, J. Chem. Phys., 136, 234309
- Fortenberry, R. C., Crawford, T. D., & Lee, J. T. 2013, ApJ, 762, 121
- Garrod, R. T., & Herbst, E. 2006, A&A, 457, 927
- Garrod, R. T., Wakelam, V. & Herbst, E., 2007, A&A, 467, 1103
- Garrod, R. T., Weaver, S. L. W., & Herbst, E., 2008, ApJ, 682, 283
- Glaser, R., Hodgen, B., Farrelly, D., & McKee, E., 2007, Astrobiol., 7, 455
- Georgievskii, Y., Klippenstein, S. J., 2005, The Journal of Chemical Physics, 122, 194103
- George, W. O., Houston, T. E., Harris, W. C., 1974, Spectrochim Acta Part A, 30, 1035
- Gupta, V.R., Tandon, P., Rawat, P., Singh, R.N. & Singh, A., 2011, A&A, 528, A129
- Herbst, E., 1987, ApJ, 313, 867
- Herbst, E. 2006, in Springer Handbook of Atomic, Molecular, and Optical Physics, ed. G. W. F. Drake (New York: Springer), 561
- Huang, X., & Lee, T. J. 2008, J. Chem. Phys., 129, 044312
- Huang, X., & Lee, T. J. 2009, J. Chem. Phys., 131, 104301
- Huang, X., & Lee, T. J. 2011, ApJ, 736, 33
- Hasegawa, T., Herbst, E., Leung, C.M., 1992, APJ, 82, 167
- Inostroza, N., Huang, X., & Lee, T. J. 2011, J. Chem. Phys., 135, 244310
- Kisiel, Z., Biakowska-J. E., Pszczkowski L., 1998, J. Chem. Phys., 109, 10263
- Kisiel, Z., Biakowska-J. E., Pszczkowski L., 2000, J. Mol. Spectrosc., 199, 5
- Kleiner, I., Godefroid, M., Herman, M., and McKellar, A. R. W., 1990, J. Mol. Spectrosc. 142, 238
- Lee, C., Yang, W., & Parr, R. G. 1988, Phys. Rev. B, 58, 785
- Le Petit, F., Roueff, E., & Herbst, E. 2004, A&A, 417, 993
- Lide, D. R., 2001, CRC Handbook of Chemistry and Physics, 82th ed.; CRC Press: Boca Raton, FL, Section 10
- Linsky, J.L., Diplas, A., Wood, B.E., Brown, A., Ayres, T.R., Savage, B.D., 1995, ApJ, 451, 335B351
- Ladd, F.E. & Covey, K.R., 2000, ApJ, 536, 380
- Lovas, F.J., Johnson, D.R., Buhl, D., Snyder, L. E., 1976, ApJ, 209, 770
- Majumdar, L., Das, A., Chakrabarti, S.K., 2014, A&A, 562, A56
- Majumdar, L., Das, A., Chakrabarti, S.K., 2014, ApJ, 782, 73
- Majumdar, L., Das, A., Chakrabarti, S.K., Chakrabarti, S., 2013a, New Astronomy, 20, 15
- Majumdar, L., Das, A., Chakrabarti, S.K., Chakrabarti, S., 2012, Research in Astronomy & Astrophysics, 12, 1613
- McKean, D., Craig, N., Law, M. 2008, J. Phys. Chem. A, 112, 6760
- Müller, H. S. P., Schloder, F., Stutzki, J., & Winnewisser, G. 2005, J. Mol. Struct., 742, 215
- Muller, H. S. P., Thorwirth, S., Roth, D. A., & Winnewisser, G. 2001, A&A, 370, L49
- Nguyen, H. V. L., Kleiner, I., Shipman, T. S., Mae, Y., Hirose, K., Hatanaka, S., Kobayashi, K., 2014, J. Mol. Spectrosc., 299, 17
- Oro, J., 1961, Nature, 190, 389
- Oro, J., Holzer, G., & Lazcano-Araujo, A., 1979, Experimental Approaches to Comets LPI Contribution 361, Ed. J. Oro, (Lunar and Planetary Institute: Texas), 54.
- Peterson, K. A., & Dunning, T. H. 2002, J. Chem. Phys., 117, 10548
- Pickett, H. M., J. Mol. Spectrosc., 1991, 148, 371
- Puletti F., Malloci G., Mulas G., Cecchi-Pestellini C., 2010, MNRAS, 402, 1667
- Pieve, F. Da, Avendano-Franco, G., Proft, F. De, Geerlings, P., 2014, MNRAS, 440, 494

- Roberts, H., Millar, T. J., 2000, A&A, 361, 388
- Runge, E., Gross, E. K. U., 1984, Phys. Rev. Lett., 52, 997
- Sahu, D., Das, A., Majumdar, L., Chakrabarti, S. K., 2015, New Astronomy, 38, 23
- Sarafian, A. R., Nielson, S.G., Marschall, H.R., McCubbin, F.M., Monteleone, B.D., 2014, Science, 346, 623
- Senent, M. L., Dominguez-Gomez, R., Carvajal, M., Kleiner, 2013, JCP, 138, 044319
- Shalabiea, O. M., Greenberg, J. M., 1994, A&A, 290, 266
- Siporska, A., Szydlowski, J., 2008, Macromolecules, 41, 4534
- Sivaraman, B., Narayanan, R., Das, A., Gopakumar, G., Majumdar, L., Chakrabarti, S. K., Subramanian, K. P., Raja Sekhar, B. N., Hada, M., 2015, MNRAS, 448, 1372
- Sivaraman, B., Nair, B. G., Lo, J. I., et al., 2013, ApJ, 778, 157
- Sivaraman, B., Mukherjee, R., 2014, Chemical Physics Letters, 33, 603
- Su, T., & Chesnavich, W. J. 1982, J. Chem. Phys., 76, 5183
- Smith I.W.M., 2006, Angewandte Chemie - International Edition, 45, 2842
- Smith I.W.M., 2011, ARA&A, 49, 29
- Tercero, B., Kleiner, I., Cernicharo, J., Nguyen, H. V. L., Lopez, A., & Munoz Caro, G. M., 2013, ApJ, 770, L13
- Tudorje, M., Kleiner, I., Hougen, J.T., Melandri, S., Sutikdja, L.W., Stahl, W., 2011, J. Mol. Spectrosc. 269, 211
- van Dishoeck, E. F., & Black, J. H. 1986, ApJS, 62, 109
- Viti, S., Collings, M. P., Dever, J. W., McCoustra, M. R. S., & Williams, D. A. 2004, MNRAS, 354, 1141
- Wakelam, V., Smith, I W. M., Herbst, E. et al., 2010, Space Sci. Rev., 156, 13
- Watson, J. 1977, Vibrational Spectra and Structure., ed. J. Durig (Amsterdam: Elsevier), 8, 1
- Woon, D. E., Herbst, E., 2009, APJS, 185, 273
- Woodall, J., Agndez, M., Markwick-Kemper, A.J., Millar, T.J., 2007, A&A, 466, 1197

TABLE 8
ROTATIONAL TRANSITIONS FOR GAS PHASE CH₃COOCH₂D

Frequency ^a (in MHz)	I ^c	D ^d	E _{lower} ^e (in cm ⁻¹)	g _{up} ^f	Tag ^g	QnF ^h	Upper state (Qn _{up} ⁱ)	Lower state (Qn _{lower} ^j)
6870.0333	-8.3550	3	-0.0000	1	74003	304	1 0 1 0	0 0 0 1
6870.0524	-7.6560	3	-0.0000	5	74003	304	1 0 1 2	0 0 0 1
6870.0651	-7.8779	3	-0.0000	3	74003	304	1 0 1 1	0 0 0 1
13740.0730	-7.5775	3	0.2292	3	74003	304	2 0 2 1	1 0 1 1
13740.0857	-8.7536	3	0.2292	3	74003	304	2 0 2 1	1 0 1 2
13740.0932	-6.8294	3	0.2292	7	74003	304	2 0 2 3	1 0 1 2
13740.0942	-7.1004	3	0.2292	5	74003	304	2 0 2 2	1 0 1 1
13740.1047	-7.4526	3	0.2292	3	74003	304	2 0 2 1	1 0 1 0
13740.1069	-7.5775	3	0.2292	5	74003	304	2 0 2 2	1 0 1 2
20610.0850	-7.4027	3	0.6875	5	74003	304	3 0 3 2	2 0 2 2
20610.0986	-8.9467	3	0.6875	5	74003	304	3 0 3 2	2 0 2 3
20610.1035	-6.3393	3	0.6875	9	74003	304	3 0 3 4	2 0 2 3
20610.1040	-6.4996	3	0.6875	7	74003	304	3 0 3 3	2 0 2 2
20610.1061	-6.6703	3	0.6875	5	74003	304	3 0 3 2	2 0 2 1
20610.1176	-7.4027	3	0.6875	7	74003	304	3 0 3 3	2 0 2 3
27480.0511	-7.2794	3	1.3750	7	74003	304	4 0 4 3	3 0 3 3
27480.0689	-5.9881	3	1.3750	11	74003	304	4 0 4 5	3 0 3 4
27480.0692	-6.1033	3	1.3750	9	74003	304	4 0 4 4	3 0 3 3
27480.0701	-6.2214	3	1.3750	7	74003	304	4 0 4 3	3 0 3 2
27480.0833	-7.2794	3	1.3750	9	74003	304	4 0 4 4	3 0 3 4
34349.9572	-7.1846	3	2.2916	9	74003	304	5 0 5 4	4 0 4 4
34349.9747	-5.7141	3	2.2916	13	74003	304	5 0 5 6	4 0 4 5
34349.9749	-5.8044	3	2.2916	11	74003	304	5 0 5 5	4 0 4 4
34349.9754	-5.8958	3	2.2916	9	74003	304	5 0 5 4	4 0 4 3
34349.9893	-7.1846	3	2.2916	11	74003	304	5 0 5 5	4 0 4 5
41219.7888	-7.1081	3	3.4374	11	74003	304	6 0 6 5	5 0 5 5
41219.8060	-5.4896	3	3.4374	15	74003	304	6 0 6 7	5 0 5 6
41219.8061	-5.5640	3	3.4374	13	74003	304	6 0 6 6	5 0 5 5
41219.8064	-5.6389	3	3.4374	11	74003	304	6 0 6 5	5 0 5 4
41219.8208	-7.1081	3	3.4374	13	74003	304	6 0 6 6	5 0 5 6
48089.5309	-7.0442	3	4.8123	13	74003	304	7 0 7 6	6 0 6 6
48089.5479	-5.2997	3	4.8123	17	74003	304	7 0 7 8	6 0 6 7
48089.5480	-5.3630	3	4.8123	15	74003	304	7 0 7 7	6 0 6 6
48089.5483	-5.4266	3	4.8123	13	74003	304	7 0 7 6	6 0 6 5
48089.5629	-7.0442	3	4.8123	15	74003	304	7 0 7 7	6 0 6 7
54959.1688	-6.9898	3	6.4164	15	74003	304	8 0 8 7	7 0 7 7
54959.1857	-5.1353	3	6.4164	19	74003	304	8 0 8 9	7 0 7 8
54959.1858	-5.1905	3	6.4164	17	74003	304	8 0 8 8	7 0 7 7
54959.1859	-5.2458	3	6.4164	15	74003	304	8 0 8 7	7 0 7 6
54959.2007	-6.9898	3	6.4164	17	74003	304	8 0 8 8	7 0 7 8
61828.6876	-6.9427	3	8.2497	17	74003	304	9 0 9 8	8 0 8 8
61828.7043	-4.9908	3	8.2497	21	74003	304	9 0 9 10	8 0 8 9
61828.7044	-5.0396	3	8.2497	19	74003	304	9 0 9 9	8 0 8 8
61828.7045	-5.0886	3	8.2497	17	74003	304	9 0 9 8	8 0 8 7
61828.7195	-6.9427	3	8.2497	19	74003	304	9 0 9 9	8 0 8 9
68698.0724	-6.9015	3	10.3121	19	74003	304	10 0 10 9	9 0 9 9
68698.0890	-4.8620	3	10.3121	23	74003	304	10 0 10 11	9 0 9 10
68698.0891	-4.9059	3	10.3121	21	74003	304	10 0 10 10	9 0 9 9
68698.0892	-4.9498	3	10.3121	19	74003	304	10 0 10 9	9 0 9 8
68698.1042	-6.9015	3	10.3121	21	74003	304	10 0 10 10	9 0 9 10
75567.3082	-6.8651	3	12.6036	21	74003	304	11 0 11 10	10 0 10 10
75567.3248	-4.7461	3	12.6036	25	74003	304	11 0 11 12	10 0 10 11
75567.3249	-4.7860	3	12.6036	23	74003	304	11 0 11 11	10 0 10 10
75567.3250	-4.8258	3	12.6036	21	74003	304	11 0 11 10	10 0 10 9
75567.3401	-6.8651	3	12.6036	23	74003	304	11 0 11 11	10 0 10 11
82436.3804	-6.8328	3	15.1242	23	74003	304	12 0 12 11	11 0 11 11
82436.3969	-4.6411	3	15.1242	27	74003	304	12 0 12 13	11 0 11 12
82436.3970	-4.7140	3	15.1242	23	74003	304	12 0 12 11	11 0 11 10
82436.3970	-4.6775	3	15.1242	25	74003	304	12 0 12 12	11 0 11 11
82436.4122	-6.8328	3	15.1242	25	74003	304	12 0 12 12	11 0 11 12
89305.2739	-6.8041	3	17.8740	25	74003	304	13 0 13 12	12 0 12 12
89305.2904	-4.5787	3	17.8740	27	74003	304	13 0 13 13	12 0 12 12
89305.2904	-4.5451	3	17.8740	29	74003	304	13 0 13 14	12 0 12 13
89305.2905	-4.6124	3	17.8740	25	74003	304	13 0 13 12	12 0 12 11
89305.3057	-6.8041	3	17.8740	27	74003	304	13 0 13 13	12 0 12 13
96173.9739	-6.7783	3	20.8529	27	74003	304	14 0 14 13	13 0 13 13
96173.9903	-4.4883	3	20.8529	29	74003	304	14 0 14 14	13 0 13 13
96173.9903	-4.4571	3	20.8529	31	74003	304	14 0 14 15	13 0 13 14
96173.9904	-4.5195	3	20.8529	27	74003	304	14 0 14 13	13 0 13 12
96174.0057	-6.7783	3	20.8529	29	74003	304	14 0 14 14	13 0 13 14

Frequency ^a (in MHz)	I ^c	D ^d	E _{lower} ^e (in cm ⁻¹)	g _{up} ^f	Tag ^g	QnF ^h	Upper state (Qn _{up} ⁱ)	Lower state (Qn _{lower} ^j)
103042.4654	-6.7553	3	24.0609	29	74003	304	15 01514	14 01414
103042.4819	-4.4341	3	24.0609	29	74003	304	15 01514	14 01413
103042.4819	-4.4050	3	24.0609	31	74003	304	15 01515	14 01414
103042.4819	-4.3760	3	24.0609	33	74003	304	15 01516	14 01415
103042.4973	-6.7553	3	24.0609	31	74003	304	15 01515	14 01415
109910.7337	-6.7347	3	27.4981	31	74003	304	16 01615	15 01515
109910.7501	-4.3281	3	27.4981	33	74003	304	16 01616	15 01515
109910.7501	-4.3009	3	27.4981	35	74003	304	16 01617	15 01516
109910.7502	-4.3554	3	27.4981	31	74003	304	16 01615	15 01514
109910.7655	-6.7347	3	27.4981	33	74003	304	16 01616	15 01516
116778.7639	-6.7162	3	31.1643	33	74003	304	17 01716	16 01616
116778.7802	-4.2568	3	31.1643	35	74003	304	17 01717	16 01616
116778.7802	-4.2312	3	31.1643	37	74003	304	17 01718	16 01617
116778.7803	-4.2825	3	31.1643	33	74003	304	17 01716	16 01615
116778.7957	-6.7162	3	31.1643	35	74003	304	17 01717	16 01617
123646.5409	-6.6998	3	35.0596	35	74003	304	18 01817	17 01717
123646.5572	-4.1664	3	35.0596	39	74003	304	18 01819	17 01718
123646.5573	-4.2148	3	35.0596	35	74003	304	18 01817	17 01716
123646.5573	-4.1906	3	35.0596	37	74003	304	18 01818	17 01717
123646.5727	-6.6998	3	35.0596	37	74003	304	18 01818	17 01718
130514.0500	-6.6851	3	39.1840	37	74003	304	19 01918	18 01818
130514.0663	-4.1288	3	39.1840	39	74003	304	19 01919	18 01818
130514.0663	-4.1059	3	39.1840	41	74003	304	19 01920	18 01819
130514.0664	-4.1517	3	39.1840	37	74003	304	19 01918	18 01817
130514.0818	-6.6851	3	39.1840	39	74003	304	19 01919	18 01819
137381.2763	-6.6722	3	43.5375	39	74003	304	20 02019	19 01919
137381.2926	-4.0930	3	43.5375	39	74003	304	20 02019	19 01918
137381.2926	-4.0712	3	43.5375	41	74003	304	20 02020	19 01919
137381.2926	-4.0494	3	43.5375	43	74003	304	20 02021	19 01920
137381.3081	-6.6722	3	43.5375	41	74003	304	20 02020	19 01920
144248.2049	-6.6608	3	48.1200	41	74003	304	21 02120	20 02020
144248.2211	-3.9966	3	48.1200	45	74003	304	21 02122	20 02021
144248.2212	-4.0380	3	48.1200	41	74003	304	21 02120	20 02019
144248.2212	-4.0173	3	48.1200	43	74003	304	21 02121	20 02020
144248.2367	-6.6608	3	48.1200	43	74003	304	21 02121	20 02021
151114.8209	-6.6508	3	52.9316	43	74003	304	22 02221	21 02121
151114.8371	-3.9867	3	52.9316	43	74003	304	22 02221	21 02120
151114.8371	-3.9669	3	52.9316	45	74003	304	22 02222	21 02121
151114.8371	-3.9471	3	52.9316	47	74003	304	22 02223	21 02122
151114.8527	-6.6508	3	52.9316	45	74003	304	22 02222	21 02122
157981.1094	-6.6423	3	57.9723	45	74003	304	23 02322	22 02222
157981.1256	-3.9386	3	57.9723	45	74003	304	23 02322	22 02221
157981.1256	-3.9196	3	57.9723	47	74003	304	23 02323	22 02222
157981.1256	-3.9007	3	57.9723	49	74003	304	23 02324	22 02223
157981.1411	-6.6423	3	57.9723	47	74003	304	23 02323	22 02223
164847.0555	-6.6350	3	63.2420	47	74003	304	24 02423	23 02323
164847.0717	-3.8935	3	63.2420	47	74003	304	24 02423	23 02322
164847.0717	-3.8754	3	63.2420	49	74003	304	24 02424	23 02323
164847.0717	-3.8572	3	63.2420	51	74003	304	24 02425	23 02324
164847.0873	-6.6350	3	63.2420	49	74003	304	24 02424	23 02324
171712.6444	-6.6290	3	68.7407	49	74003	304	25 02524	24 02424
171712.6606	-3.8512	3	68.7407	49	74003	304	25 02524	24 02423
171712.6606	-3.8338	3	68.7407	51	74003	304	25 02525	24 02424
171712.6606	-3.8164	3	68.7407	53	74003	304	25 02526	24 02425
171712.6761	-6.6290	3	68.7407	51	74003	304	25 02525	24 02425
178577.8611	-6.6242	3	74.4684	51	74003	304	26 02625	25 02525
178577.8773	-3.8116	3	74.4684	51	74003	304	26 02625	25 02524
178577.8773	-3.7949	3	74.4684	53	74003	304	26 02626	25 02525
178577.8773	-3.7781	3	74.4684	55	74003	304	26 02627	25 02526
178577.8929	-6.6242	3	74.4684	53	74003	304	26 02626	25 02526
185442.6908	-6.6204	3	80.4251	53	74003	304	27 02726	26 02626
185442.7070	-3.7744	3	80.4251	53	74003	304	27 02726	26 02625
185442.7070	-3.7583	3	80.4251	55	74003	304	27 02727	26 02626
185442.7070	-3.7422	3	80.4251	57	74003	304	27 02728	26 02627
185442.7226	-6.6204	3	80.4251	55	74003	304	27 02727	26 02627
192307.1186	-6.6178	3	86.6108	55	74003	304	28 02827	27 02727
192307.1348	-3.7395	3	86.6108	55	74003	304	28 02827	27 02726
192307.1348	-3.7240	3	86.6108	57	74003	304	28 02828	27 02727
192307.1348	-3.7085	3	86.6108	59	74003	304	28 02829	27 02728
192307.1504	-6.6178	3	86.6108	57	74003	304	28 02828	27 02728

Frequency ^a (in MHz)	I ^c	D ^d	E _{lower} ^e (in cm ⁻¹)	g _{up} ^f	Tag ^g	QnF ^h	Upper state (Qn _{up} ⁱ)	Lower state (Qn _{lower} ^j)
199171.1296	-6.6161	3	93.0255	57	74003	304	29 02928	28 02828
199171.1457	-3.6769	3	93.0255	61	74003	304	29 02930	28 02829
199171.1458	-3.7069	3	93.0255	57	74003	304	29 02928	28 02827
199171.1458	-3.6919	3	93.0255	59	74003	304	29 02929	28 02828
199171.1614	-6.6161	3	93.0255	59	74003	304	29 02929	28 02829
206034.7089	-6.6155	3	99.6691	59	74003	304	30 03029	29 02929
206034.7251	-3.6763	3	99.6691	59	74003	304	30 03029	29 02928
206034.7251	-3.6618	3	99.6691	61	74003	304	30 03030	29 02929
206034.7251	-3.6473	3	99.6691	63	74003	304	30 03031	29 02930
206034.7407	-6.6155	3	99.6691	61	74003	304	30 03030	29 02930
212897.8417	-6.6158	3	106.5417	61	74003	304	31 03130	30 03030
212897.8578	-3.6476	3	106.5417	61	74003	304	31 03130	30 03029
212897.8578	-3.6336	3	106.5417	63	74003	304	31 03131	30 03030
212897.8578	-3.6196	3	106.5417	65	74003	304	31 03132	30 03031
212897.8734	-6.6158	3	106.5417	63	74003	304	31 03131	30 03031
219760.5130	-6.6171	3	113.6432	63	74003	304	32 03231	31 03131
219760.5291	-3.6208	3	113.6432	63	74003	304	32 03231	31 03130
219760.5291	-3.6072	3	113.6432	65	74003	304	32 03232	31 03131
219760.5291	-3.5936	3	113.6432	67	74003	304	32 03233	31 03132
219760.5447	-6.6171	3	113.6432	65	74003	304	32 03232	31 03132
226622.7079	-6.6193	3	120.9736	65	74003	304	33 03332	32 03232
226622.7240	-3.5826	3	120.9736	67	74003	304	33 03333	32 03232
226622.7240	-3.5695	3	120.9736	69	74003	304	33 03334	32 03233
226622.7241	-3.5958	3	120.9736	65	74003	304	33 03332	32 03231
226622.7397	-6.6193	3	120.9736	67	74003	304	33 03333	32 03233
233484.4117	-6.6223	3	128.5330	67	74003	304	34 03433	33 03333
233484.4278	-3.5725	3	128.5330	67	74003	304	34 03433	33 03332
233484.4278	-3.5597	3	128.5330	69	74003	304	34 03434	33 03333
233484.4278	-3.5469	3	128.5330	71	74003	304	34 03435	33 03334
233484.4434	-6.6223	3	128.5330	69	74003	304	34 03434	33 03334
240345.6093	-6.6262	3	136.3212	69	74003	304	35 03534	34 03434
240345.6254	-3.5508	3	136.3212	69	74003	304	35 03534	34 03433
240345.6254	-3.5384	3	136.3212	71	74003	304	35 03535	34 03434
240345.6254	-3.5260	3	136.3212	73	74003	304	35 03536	34 03435
240345.6411	-6.6262	3	136.3212	71	74003	304	35 03535	34 03435
247206.2859	-6.6309	3	144.3382	71	74003	304	36 03635	35 03535
247206.3020	-3.5307	3	144.3382	71	74003	304	36 03635	35 03534
247206.3020	-3.5186	3	144.3382	73	74003	304	36 03636	35 03535
247206.3020	-3.5066	3	144.3382	75	74003	304	36 03637	35 03536
247206.3177	-6.6309	3	144.3382	73	74003	304	36 03636	35 03536
254066.4267	-6.6365	3	152.5841	73	74003	304	37 03736	36 03636
254066.4428	-3.5121	3	152.5841	73	74003	304	37 03736	36 03635
254066.4428	-3.5004	3	152.5841	75	74003	304	37 03737	36 03636
254066.4428	-3.4886	3	152.5841	77	74003	304	37 03738	36 03637
254066.4584	-6.6365	3	152.5841	75	74003	304	37 03737	36 03637
260926.0167	-6.6428	3	161.0589	75	74003	304	38 03837	37 03737
260926.0327	-3.4721	3	161.0589	79	74003	304	38 03839	37 03738
260926.0328	-3.4950	3	161.0589	75	74003	304	38 03837	37 03736
260926.0328	-3.4835	3	161.0589	77	74003	304	38 03838	37 03737
260926.0484	-6.6428	3	161.0589	77	74003	304	38 03838	37 03738
267785.0410	-6.6499	3	169.7624	77	74003	304	39 03938	38 03838
267785.0571	-3.4792	3	169.7624	77	74003	304	39 03938	38 03837
267785.0571	-3.4680	3	169.7624	79	74003	304	39 03939	38 03838
267785.0571	-3.4569	3	169.7624	81	74003	304	39 03940	38 03839
267785.0728	-6.6499	3	169.7624	79	74003	304	39 03939	38 03839
274643.4848	-6.6578	3	178.6948	79	74003	304	40 04039	39 03939
274643.5009	-3.4648	3	178.6948	79	74003	304	40 04039	39 03938
274643.5009	-3.4539	3	178.6948	81	74003	304	40 04040	39 03939
274643.5009	-3.4431	3	178.6948	83	74003	304	40 04041	39 03940
274643.5166	-6.6578	3	178.6948	81	74003	304	40 04040	39 03940

Frequency ^a (in MHz)	I ^c	D ^d	E _{lower} ^e (in cm ⁻¹)	g _{up} ^f	Tag ^g	QnF ^h	Upper state (Qn _{up} ⁱ)	Lower state (Qn _{lower} ^j)
199171.1296	-6.6161	3	93.0255	57	74003	304	29 02928	28 02828
281501.3332	-6.6664	3	187.8559	81	74003	304	41 04140	40 04040
281501.3493	-3.4517	3	187.8559	81	74003	304	41 04140	40 04039
281501.3493	-3.4411	3	187.8559	83	74003	304	41 04141	40 04040
281501.3493	-3.4305	3	187.8559	85	74003	304	41 04142	40 04041
281501.3650	-6.6664	3	187.8559	83	74003	304	41 04141	40 04041
288358.5712	-6.6757	3	197.2458	83	74003	304	42 04241	41 04141
288358.5873	-3.4398	3	197.2458	83	74003	304	42 04241	41 04140
288358.5873	-3.4295	3	197.2458	85	74003	304	42 04242	41 04141
288358.5873	-3.4191	3	197.2458	87	74003	304	42 04243	41 04142
288358.6030	-6.6757	3	197.2458	85	74003	304	42 04242	41 04142
295215.1841	-6.6858	3	206.8644	85	74003	304	43 04342	42 04242
295215.2002	-3.4292	3	206.8644	85	74003	304	43 04342	42 04241
295215.2002	-3.4191	3	206.8644	87	74003	304	43 04343	42 04242
295215.2002	-3.4090	3	206.8644	89	74003	304	43 04344	42 04243
295215.2159	-6.6858	3	206.8644	87	74003	304	43 04343	42 04243

^a Calculated frequency in MHz

in units of MHz then uncertainty of the line is greater or equal to zero.

^c Base 10 logarithm of the integrated intensity at 300K in nm² MHz^d Degrees of freedom in the rotational partition function

(0 for atoms, 2 for linear molecules, 3 for non linear molecules)

^e Lower state energy in cm⁻¹ relative to the lowest energy level in the ground vibronic state.^f Upper state degeneracy : g_{up} = g_I × g_N, where g_I is the spin statistical weight and g_N = 2N + 1 the rotational degeneracy.^g Molecule Tag^h Coding for the format of quantum numbers.QnF=100 × Q + 10 × H + N_{Qn}; N_{Qn} is the number of quantum numbers for each state; H indicates the number of half integer quantum numbers; Qmod5, the residual when Q is divided by 5, gives the number of principal quantum numbers (without the spin designating ones)ⁱ Quantum numbers for the upper state^j Quantum numbers for the lower state

TABLE 9
ROTATIONAL TRANSITIONS FOR GAS PHASE CH₂DCOOCH₃

Frequency ^a (in MHz)	I ^c	D ^d	E _{lower} ^e (in cm ⁻¹)	g _{up} ^f	Tag ^g	QnF ^h	Upper state (Qn _{up} ⁱ)	Lower state (Qn _{lower} ^j)
6996.8647	-7.8605	3	-0.0000	3	74003	304	1 0 1 1	0 0 0 1
6996.8923	-7.6387	3	-0.0000	5	74003	304	1 0 1 2	0 0 0 1
6996.9337	-8.3376	3	-0.0000	1	74003	304	1 0 1 0	0 0 0 1
13993.7279	-7.5602	3	0.2334	5	74003	304	2 0 2 2	1 0 1 2
13993.7325	-7.4353	3	0.2334	3	74003	304	2 0 2 1	1 0 1 0
13993.7555	-7.0831	3	0.2334	5	74003	304	2 0 2 2	1 0 1 1
13993.7575	-6.8120	3	0.2334	7	74003	304	2 0 2 3	1 0 1 2
13993.7739	-8.7363	3	0.2334	3	74003	304	2 0 2 1	1 0 1 2
13993.8015	-7.5602	3	0.2334	3	74003	304	2 0 2 1	1 0 1 1
20990.5541	-7.3853	3	0.7002	7	74003	304	3 0 3 3	2 0 2 3
20990.5791	-6.6529	3	0.7002	5	74003	304	3 0 3 2	2 0 2 1
20990.5837	-6.4822	3	0.7002	7	74003	304	3 0 3 3	2 0 2 2
20990.5848	-6.3219	3	0.7002	9	74003	304	3 0 3 4	2 0 2 3
20990.5955	-8.9294	3	0.7002	5	74003	304	3 0 3 2	2 0 2 3
20990.6251	-7.3853	3	0.7002	5	74003	304	3 0 3 2	2 0 2 2
27987.3216	-7.2621	3	1.4003	9	74003	304	4 0 4 4	3 0 3 4
27987.3503	-6.2041	3	1.4003	7	74003	304	4 0 4 3	3 0 3 2
27987.3522	-6.0860	3	1.4003	9	74003	304	4 0 4 4	3 0 3 3
27987.3529	-5.9708	3	1.4003	11	74003	304	4 0 4 5	3 0 3 4
27987.3917	-7.2621	3	1.4003	7	74003	304	4 0 4 3	3 0 3 3
34984.0100	-7.1674	3	2.3339	11	74003	304	5 0 5 5	4 0 4 5
34984.0403	-5.8786	3	2.3339	9	74003	304	5 0 5 4	4 0 4 3
34984.0414	-5.7872	3	2.3339	11	74003	304	5 0 5 5	4 0 4 4
34984.0419	-5.6969	3	2.3339	13	74003	304	5 0 5 6	4 0 4 5
34984.0797	-7.1674	3	2.3339	9	74003	304	5 0 5 4	4 0 4 4
41980.5995	-7.0909	3	3.5008	13	74003	304	6 0 6 6	5 0 5 6
41980.6306	-5.6217	3	3.5008	11	74003	304	6 0 6 5	5 0 5 4
41980.6313	-5.5468	3	3.5008	13	74003	304	6 0 6 6	5 0 5 5
41980.6317	-5.4724	3	3.5008	15	74003	304	6 0 6 7	5 0 5 6
41980.6690	-7.0909	3	3.5008	11	74003	304	6 0 6 5	5 0 5 5
48977.0699	-7.0271	3	4.9012	15	74003	304	7 0 7 7	6 0 6 7
48977.1016	-5.4095	3	4.9012	13	74003	304	7 0 7 6	6 0 6 5
48977.1021	-5.3459	3	4.9012	15	74003	304	7 0 7 7	6 0 6 6
48977.1024	-5.2825	3	4.9012	17	74003	304	7 0 7 8	6 0 6 7
48977.1393	-7.0271	3	4.9012	13	74003	304	7 0 7 6	6 0 6 6
55973.4014	-6.9728	3	6.5349	17	74003	304	8 0 8 8	7 0 7 8
55973.4336	-5.2287	3	6.5349	15	74003	304	8 0 8 7	7 0 7 6
55973.4339	-5.1734	3	6.5349	17	74003	304	8 0 8 8	7 0 7 7
55973.4341	-5.1183	3	6.5349	19	74003	304	8 0 8 9	7 0 7 8
55973.4707	-6.9728	3	6.5349	15	74003	304	8 0 8 7	7 0 7 7
62969.5742	-6.9257	3	8.4019	19	74003	304	9 0 9 9	8 0 8 9
62969.6067	-5.0716	3	8.4019	17	74003	304	9 0 9 8	8 0 8 7
62969.6069	-5.0227	3	8.4019	19	74003	304	9 0 9 9	8 0 8 8
62969.6071	-4.9738	3	8.4019	21	74003	304	9 0 9 10	8 0 8 9
62969.6435	-6.9257	3	8.4019	17	74003	304	9 0 9 8	8 0 8 8
69965.5684	-6.8846	3	10.5024	21	74003	304	10 0 10 10	9 0 9 10
69965.6010	-4.9329	3	10.5024	19	74003	304	10 0 10 9	9 0 9 8
69965.6013	-4.8890	3	10.5024	21	74003	304	10 0 10 10	9 0 9 9
69965.6014	-4.8451	3	10.5024	23	74003	304	10 0 10 11	9 0 9 10
69965.6376	-6.8846	3	10.5024	19	74003	304	10 0 10 9	9 0 9 9
76961.3641	-6.8483	3	12.8362	23	74003	304	11 0 11 11	10 0 10 11
76961.3969	-4.8090	3	12.8362	21	74003	304	11 0 11 10	10 0 10 9
76961.3971	-4.7691	3	12.8362	23	74003	304	11 0 11 11	10 0 10 10
76961.3972	-4.7293	3	12.8362	25	74003	304	11 0 11 12	10 0 10 11
76961.4332	-6.8483	3	12.8362	21	74003	304	11 0 11 10	10 0 10 10
83956.9414	-6.8161	3	15.4033	25	74003	304	12 0 12 12	11 0 11 12
83956.9744	-4.6973	3	15.4033	23	74003	304	12 0 12 11	11 0 11 10
83956.9745	-4.6608	3	15.4033	25	74003	304	12 0 12 12	11 0 11 11
83956.9746	-4.6244	3	15.4033	27	74003	304	12 0 12 13	11 0 11 12
83957.0105	-6.8161	3	15.4033	23	74003	304	12 0 12 11	11 0 11 11
90952.2805	-6.7875	3	18.2038	27	74003	304	13 0 13 13	12 0 12 13
90952.3136	-4.5958	3	18.2038	25	74003	304	13 0 13 12	12 0 12 11
90952.3137	-4.5622	3	18.2038	27	74003	304	13 0 13 13	12 0 12 12
90952.3138	-4.5285	3	18.2038	29	74003	304	13 0 13 14	12 0 12 13
90952.3496	-6.7875	3	18.2038	25	74003	304	13 0 13 12	12 0 12 12

Frequency ^a (in MHz)	I ^c	D ^d	E _{lower} ^e (in cm ⁻¹)	g _{up} ^f	Tag ^g	QnF ^h	Upper state (Qn _{up} ⁱ)	Lower state (Qn _{lower} ^j)
97947.3615	-6.7619	3	21.2377	29	74003	304	14 01414	13 01314
97947.3947	-4.5030	3	21.2377	27	74003	304	14 01413	13 01312
97947.3948	-4.4718	3	21.2377	29	74003	304	14 01414	13 01313
97947.3949	-4.4406	3	21.2377	31	74003	304	14 01415	13 01314
97947.4306	-6.7619	3	21.2377	27	74003	304	14 01413	13 01313
104942.1646	-6.7389	3	24.5049	31	74003	304	15 01515	14 01415
104942.1979	-4.4178	3	24.5049	29	74003	304	15 01514	14 01413
104942.1980	-4.3887	3	24.5049	31	74003	304	15 01515	14 01414
104942.1981	-4.3596	3	24.5049	33	74003	304	15 01516	14 01415
104942.2337	-6.7389	3	24.5049	29	74003	304	15 01514	14 01414
111936.6699	-6.7185	3	28.0054	33	74003	304	16 01616	15 01516
111936.7033	-4.3392	3	28.0054	31	74003	304	16 01615	15 01514
111936.7034	-4.3119	3	28.0053	33	74003	304	16 01616	15 01515
111936.7035	-4.2847	3	28.0054	35	74003	304	16 01617	15 01516
111936.7390	-6.7185	3	28.0053	31	74003	304	16 01615	15 01515
118930.8576	-6.7002	3	31.7392	35	74003	304	17 01717	16 01617
118930.8911	-4.2664	3	31.7392	33	74003	304	17 01716	16 01615
118930.8912	-4.2408	3	31.7392	35	74003	304	17 01717	16 01616
118930.8912	-4.2151	3	31.7392	37	74003	304	17 01718	16 01617
118930.9267	-6.7002	3	31.7392	33	74003	304	17 01716	16 01616
125924.7079	-6.6839	3	35.7063	37	74003	304	18 01818	17 01718
125924.7414	-4.1989	3	35.7063	35	74003	304	18 01817	17 01716
125924.7414	-4.1747	3	35.7063	37	74003	304	18 01818	17 01717
125924.7415	-4.1505	3	35.7063	39	74003	304	18 01819	17 01718
125924.7769	-6.6839	3	35.7063	35	74003	304	18 01817	17 01717
132918.2007	-6.6694	3	39.9067	39	74003	304	19 01919	18 01819
132918.2343	-4.1360	3	39.9067	37	74003	304	19 01918	18 01817
132918.2344	-4.1131	3	39.9067	39	74003	304	19 01919	18 01818
132918.2344	-4.0902	3	39.9067	41	74003	304	19 01920	18 01819
132918.2698	-6.6694	3	39.9067	37	74003	304	19 01918	18 01818
139911.3164	-6.6566	3	44.3403	41	74003	304	20 02020	19 01920
139911.3500	-4.0774	3	44.3403	39	74003	304	20 02019	19 01918
139911.3501	-4.0556	3	44.3403	41	74003	304	20 02020	19 01919
139911.3501	-4.0339	3	44.3403	43	74003	304	20 02021	19 01920
139911.3855	-6.6566	3	44.3403	39	74003	304	20 02019	19 01919
146904.0351	-6.6454	3	49.0073	43	74003	304	21 02121	20 02021
146904.0687	-4.0227	3	49.0073	41	74003	304	21 02120	20 02019
146904.0688	-4.0019	3	49.0073	43	74003	304	21 02121	20 02020
146904.0688	-3.9812	3	49.0073	45	74003	304	21 02122	20 02021
146904.1041	-6.6454	3	49.0073	41	74003	304	21 02120	20 02020
153896.3368	-6.6357	3	53.9075	45	74003	304	22 02222	21 02122
153896.3705	-3.9715	3	53.9075	43	74003	304	22 02221	21 02120
153896.3705	-3.9517	3	53.9075	45	74003	304	22 02222	21 02121
153896.3706	-3.9319	3	53.9075	47	74003	304	22 02223	21 02122
153896.4059	-6.6357	3	53.9075	43	74003	304	22 02221	21 02121
160888.2018	-6.6273	3	59.0409	47	74003	304	23 02323	22 02223
160888.2355	-3.9236	3	59.0409	45	74003	304	23 02322	22 02221
160888.2356	-3.9047	3	59.0409	47	74003	304	23 02323	22 02222
160888.2356	-3.8858	3	59.0409	49	74003	304	23 02324	22 02223
160888.2708	-6.6273	3	59.0409	45	74003	304	23 02322	22 02222
167879.6102	-6.6203	3	64.4076	49	74003	304	24 02424	23 02324
167879.6440	-3.8787	3	64.4076	47	74003	304	24 02423	23 02322
167879.6440	-3.8606	3	64.4076	49	74003	304	24 02424	23 02323
167879.6440	-3.8425	3	64.4076	51	74003	304	24 02425	23 02324
167879.6792	-6.6203	3	64.4076	47	74003	304	24 02423	23 02323
174870.5421	-6.6145	3	70.0074	51	74003	304	25 02525	24 02425
174870.5759	-3.8367	3	70.0074	49	74003	304	25 02524	24 02423
174870.5760	-3.8193	3	70.0074	51	74003	304	25 02525	24 02424
174870.5760	-3.8019	3	70.0074	53	74003	304	25 02526	24 02425
174870.6112	-6.6145	3	70.0074	49	74003	304	25 02524	24 02424
181860.9777	-6.6098	3	75.8405	53	74003	304	26 02626	25 02526
181861.0116	-3.7973	3	75.8405	51	74003	304	26 02625	25 02524
181861.0116	-3.7805	3	75.8405	53	74003	304	26 02626	25 02525
181861.0116	-3.7638	3	75.8405	55	74003	304	26 02627	25 02526
181861.0468	-6.6098	3	75.8405	51	74003	304	26 02625	25 02525
188850.8972	-6.6063	3	81.9067	55	74003	304	27 02727	26 02627
188850.9311	-3.7603	3	81.9067	53	74003	304	27 02726	26 02625
188850.9311	-3.7442	3	81.9067	55	74003	304	27 02727	26 02626
188850.9311	-3.7281	3	81.9067	57	74003	304	27 02728	26 02627
188850.9662	-6.6063	3	81.9067	53	74003	304	27 02726	26 02626

Frequency ^a (in MHz)	I ^c	D ^d	E _{lower} ^e (in cm ⁻¹)	g _{up} ^f	Tag ^g	QnF ^h	Upper state (Qn _{up} ⁱ)	Lower state (Qn _{lower} ^j)
195840.2807	-6.6039	3	88.2061	57	74003	304	28 02828	27 02728
195840.3145	-3.7257	3	88.2061	55	74003	304	28 02827	27 02726
195840.3146	-3.7102	3	88.2061	57	74003	304	28 02828	27 02727
195840.3146	-3.6946	3	88.2061	59	74003	304	28 02829	27 02728
195840.3497	-6.6039	3	88.2061	55	74003	304	28 02827	27 02727
202829.1082	-6.6026	3	94.7386	59	74003	304	29 02929	28 02829
202829.1421	-3.6933	3	94.7386	57	74003	304	29 02928	28 02827
202829.1422	-3.6783	3	94.7386	59	74003	304	29 02929	28 02828
202829.1422	-3.6633	3	94.7386	61	74003	304	29 02930	28 02829
202829.1773	-6.6026	3	94.7386	57	74003	304	29 02928	28 02828
209817.3601	-6.6022	3	101.5043	61	74003	304	30 03030	29 02930
209817.3940	-3.6629	3	101.5043	59	74003	304	30 03029	29 02928
209817.3940	-3.6484	3	101.5043	61	74003	304	30 03030	29 02929
209817.3941	-3.6339	3	101.5043	63	74003	304	30 03031	29 02930
209817.4291	-6.6022	3	101.5043	59	74003	304	30 03029	29 02929
216805.0164	-6.6028	3	108.5030	63	74003	304	31 03131	30 03031
216805.0503	-3.6346	3	108.5030	61	74003	304	31 03130	30 03029
216805.0504	-3.6205	3	108.5030	63	74003	304	31 03131	30 03030
216805.0504	-3.6065	3	108.5030	65	74003	304	31 03132	30 03031
216805.0854	-6.6028	3	108.5030	61	74003	304	31 03130	30 03030
223792.0573	-6.6043	3	115.7349	65	74003	304	32 03232	31 03132
223792.0912	-3.6081	3	115.7349	63	74003	304	32 03231	31 03130
223792.0912	-3.5945	3	115.7349	65	74003	304	32 03232	31 03131
223792.0913	-3.5809	3	115.7349	67	74003	304	32 03233	31 03132
223792.1263	-6.6043	3	115.7349	63	74003	304	32 03231	31 03131
230778.4629	-6.6068	3	123.1998	67	74003	304	33 03333	32 03233
230778.4968	-3.5833	3	123.1998	65	74003	304	33 03332	32 03231
230778.4968	-3.5702	3	123.1998	67	74003	304	33 03333	32 03232
230778.4969	-3.5570	3	123.1998	69	74003	304	33 03334	32 03233
230778.5319	-6.6068	3	123.1998	65	74003	304	33 03332	32 03232
237764.2133	-6.6101	3	130.8977	69	74003	304	34 03434	33 03334
237764.2473	-3.5603	3	130.8977	67	74003	304	34 03433	33 03332
237764.2473	-3.5476	3	130.8977	69	74003	304	34 03434	33 03333
237764.2473	-3.5348	3	130.8977	71	74003	304	34 03435	33 03334
237764.2823	-6.6101	3	130.8977	67	74003	304	34 03433	33 03333
244749.2888	-6.6143	3	138.8287	71	74003	304	35 03535	34 03435
244749.3228	-3.5390	3	138.8287	69	74003	304	35 03534	34 03433
244749.3228	-3.5266	3	138.8287	71	74003	304	35 03535	34 03434
244749.3228	-3.5141	3	138.8287	73	74003	304	35 03536	34 03435
244749.3578	-6.6143	3	138.8287	69	74003	304	35 03534	34 03434
251733.6694	-6.6194	3	146.9926	73	74003	304	36 03636	35 03536
251733.7035	-3.5192	3	146.9926	71	74003	304	36 03635	35 03534
251733.7035	-3.5071	3	146.9926	73	74003	304	36 03636	35 03535
251733.7035	-3.4950	3	146.9926	75	74003	304	36 03637	35 03536
251733.7385	-6.6194	3	146.9926	71	74003	304	36 03635	35 03535
258717.3354	-6.6252	3	155.3896	75	74003	304	37 03737	36 03637
258717.3694	-3.5009	3	155.3896	73	74003	304	37 03736	36 03635
258717.3694	-3.4892	3	155.3896	75	74003	304	37 03737	36 03636
258717.3695	-3.4774	3	155.3896	77	74003	304	37 03738	36 03637
258717.4044	-6.6252	3	155.3896	73	74003	304	37 03736	36 03636

Frequency ^a (in MHz)	I ^c	D ^d	E _{lower} ^e (in cm ⁻¹)	g _{up} ^f	Tag ^g	QnF ^h	Upper state (Qn _{up} ⁱ)	Lower state (Qn _{lower} ^j)
265700.2668	-6.6319	3	164.0194	77	74003	304	38 03838	37 03738
265700.3009	-3.4841	3	164.0194	75	74003	304	38 03837	37 03736
265700.3009	-3.4726	3	164.0194	77	74003	304	38 03838	37 03737
265700.3009	-3.4612	3	164.0194	79	74003	304	38 03839	37 03738
265700.3358	-6.6319	3	164.0194	75	74003	304	38 03837	37 03737
272682.4438	-6.6394	3	172.8823	79	74003	304	39 03939	38 03839
272682.4779	-3.4687	3	172.8823	77	74003	304	39 03938	38 03837
272682.4779	-3.4575	3	172.8822	79	74003	304	39 03939	38 03838
272682.4779	-3.4464	3	172.8823	81	74003	304	39 03940	38 03839
272682.5129	-6.6394	3	172.8822	77	74003	304	39 03938	38 03838
279663.8466	-6.6476	3	181.9780	81	74003	304	40 04040	39 03940
279663.8807	-3.4546	3	181.9780	79	74003	304	40 04039	39 03938
279663.8807	-3.4437	3	181.9780	81	74003	304	40 04040	39 03939
279663.8807	-3.4329	3	181.9780	83	74003	304	40 04041	39 03940
279663.9156	-6.6476	3	181.9780	79	74003	304	40 04039	39 03939
286644.4553	-6.6566	3	191.3065	83	74003	304	41 04141	40 04041
286644.4894	-3.4418	3	191.3065	81	74003	304	41 04140	40 04039
286644.4894	-3.4312	3	191.3065	83	74003	304	41 04141	40 04040
286644.4894	-3.4206	3	191.3065	85	74003	304	41 04142	40 04041
286644.5243	-6.6566	3	191.3065	81	74003	304	41 04140	40 04040
293624.2500	-6.6663	3	200.8680	85	74003	304	42 04242	41 04142
293624.2841	-3.4304	3	200.8680	83	74003	304	42 04241	41 04140
293624.2841	-3.4200	3	200.8680	85	74003	304	42 04242	41 04141
293624.2842	-3.4097	3	200.8680	87	74003	304	42 04243	41 04142
293624.3191	-6.6663	3	200.8680	83	74003	304	42 04241	41 04141

^a Calculated frequency in MHz
in units of MHz then uncertainty of the line is greater or equal to zero.
^c Base 10 logarithm of the integrated intensity at 300K in nm² MHz
^d Degrees of freedom in the rotational partition function
(0 for atoms, 2 for linear molecules, 3 for non linear molecules)
^e Lower state energy in cm⁻¹ relative to the lowest energy
level in the ground vibronic state.
^f Upper state degeneracy : g_{up} = g_I × g_N, where g_I
is the spin statistical weight and g_N = 2N + 1 the rotational degeneracy.
^g Molecule Tag
^h Coding for the format of quantum numbers.
QnF=100 × Q + 10 × H + N_{Qn}; N_{Qn} is the number of quantum
numbers for each state; H indicates the number of half integer quantum numbers;
Qmod5, the residual when Q is divided by 5, gives the number of principal
quantum numbers (without the spin designating ones)
ⁱ Quantum numbers for the upper state
^j Quantum numbers for the lower state